Impact of aerosols on the OMI tropospheric NO2 retrievals over industrialized regions how accurate is the aerosol correction of cloud-free scenes via a simple cloud model?

Chimot, JJ; Vlemmix, T; Veefkind, JP; de Haan, J.F; Levelt, PF

DOI
10.5194/amt-9-359-2016

Publication date
2016

Document Version
Final published version

Published in
Atmospheric Measurement Techniques

Atmos. Meas. Tech., 9, 359–382, 2016
www.atmos-meas-tech.net/9/359/2016/
doi:10.5194/amt-9-359-2016

Atmospheric Measurement Techniques
Open Access
EGU

Impact of aerosols on the OMI tropospheric NO_2 retrievals over industrialized regions: how accurate is the aerosol correction of cloud-free scenes via a simple cloud model?

J. Chimot[1], T. Vlemmix[1], J. P. Veefkind[1,2], J. F. de Haan[2], and P. F. Levelt[1,2]

[1]Department of Geoscience and Remote Sensing (GRS), Civil Engineering and Geosciences, TU Delft, Delft, the Netherlands
[2]Royal Netherlands Meteorological Institute, De Bilt, the Netherlands

Correspondence to: J. Chimot (j.j.chimot@tudelft.nl)

Received: 3 June 2015 – Published in Atmos. Meas. Tech. Discuss.: 10 August 2015
Revised: 15 January 2016 – Accepted: 21 January 2016 – Published: 5 February 2016

Abstract. The Ozone Monitoring Instrument (OMI) has provided daily global measurements of tropospheric NO_2 for more than a decade. Numerous studies have drawn attention to the complexities related to measurements of tropospheric NO_2 in the presence of aerosols. Fine particles affect the OMI spectral measurements and the length of the average light path followed by the photons. However, they are not explicitly taken into account in the current operational OMI tropospheric NO_2 retrieval chain (DOMINO – Derivation of OMI tropospheric NO_2) product. Instead, the operational OMI $O_2{-}O_2$ cloud retrieval algorithm is applied both to cloudy and to cloud-free scenes (i.e. clear sky) dominated by the presence of aerosols. This paper describes in detail the complex interplay between the spectral effects of aerosols in the satellite observation and the associated response of the OMI $O_2{-}O_2$ cloud retrieval algorithm. Then, it evaluates the impact on the accuracy of the tropospheric NO_2 retrievals through the computed Air Mass Factor (AMF) with a focus on cloud-free scenes. For that purpose, collocated OMI NO_2 and MODIS (Moderate Resolution Imaging Spectroradiometer) Aqua aerosol products are analysed over the strongly industrialized East China area. In addition, aerosol effects on the tropospheric NO_2 AMF and the retrieval of OMI cloud parameters are simulated. Both the observation-based and the simulation-based approach demonstrate that the retrieved cloud fraction increases with increasing Aerosol Optical Thickness (AOT), but the magnitude of this increase depends on the aerosol properties and surface albedo. This increase is induced by the additional scattering effects of aerosols which enhance the scene brightness. The decreasing effective cloud pressure with increasing AOT primarily represents the shielding effects of the $O_2{-}O_2$ column located below the aerosol layers. The study cases show that the aerosol correction based on the implemented OMI cloud model results in biases between -20 and -40 % for the DOMINO tropospheric NO_2 product in cases of high aerosol pollution (AOT ≥ 0.6) at elevated altitude. These biases result from a combination of the cloud model error, used in the presence of aerosols, and the limitations of the current OMI cloud Look-Up-Table (LUT). A new LUT with a higher sampling must be designed to remove the complex behaviour between these biases and AOT. In contrast, when aerosols are relatively close to the surface or mixed with NO_2, aerosol correction based on the cloud model results in an overestimation of the DOMINO tropospheric NO_2 column, between 10 and 20 %. These numbers are in line with comparison studies between ground-based and OMI tropospheric NO_2 measurements in the presence of high aerosol pollution and particles located at higher altitudes. This highlights the need to implement an improved aerosol correction in the computation of tropospheric NO_2 AMFs.

1 Introduction

Nitrogen oxides ($NO_x = NO + NO_2$) play a key role in atmospheric chemistry, regulating the level of ozone and maintaining the oxidizing capacity in the troposphere. The most

important reasons to improve our knowledge of the global distributions of NO_x are (1) exposure to nitrogen dioxide leads to adverse health impacts; (2) the chemical budget of tropospheric ozone, also toxic for humans and the vegetation, is largely determined by the concentration of NO_x (Jacob et al., 2006); (3) nitrogen oxides are the precursors of (ammonium) nitrate, an important component of particulate matter, and contribute to acidification and eutrophication of soils and surface waters; and (4) nitrogen oxides affect the global climate indirectly by affecting OH, and therefore modifying the residence time of the greenhouse gases O_3 and CH_4 (Shindell et al., 2009).

In 2004, the Dutch–Finnish Ozone Monitoring Instrument (OMI) (Levelt et al., 2006) was launched on the NASA EOS-Aura (National Aeronautics and Space Administration Earth Observing System) satellite. OMI is a nadir-viewing imaging spectrometer that provides with daily global coverage of key air quality components. The retrieval technique of the OMI tropospheric NO_2 Vertical Column Density (VCD) (Boersma et al., 2004) is common to all the other similar satellite missions (Burrows et al., 1999; Bovensmann et al., 1999). The backscattered solar radiation is captured in daylight in the visible spectral domain by the instrument at the Top Of the Atmosphere (TOA) and then processed through the Differential Optical Absorption Spectroscopy (DOAS) retrieval approach. The DOAS method is based on radiative transfer modelling of tropospheric NO_2 Air Mass Factor (AMF). The associated assumptions play a crucial role in the accuracy of the tropospheric NO_2 VCD.

The DOMINO (Derivation of OMI tropospheric NO_2) (Boersma et al., 2011) product contains worldwide concentrations of NO_2 in the troposphere derived from OMI. This product is used by a large number of air quality studies (e.g. Curier et al., 2014; Reuter et al., 2014; Ding et al., 2015). The computation of tropospheric NO_2 AMF is acknowledged as the dominant source of errors in the retrieved tropospheric NO_2 column over polluted areas (Boersma et al., 2007) with important consequences for emission constraints and other applications. The overall uncertainty of the latest version of individual retrieved DOMINO tropospheric NO_2 vertical column densities is estimated to be 1.0×10^{15} molecules cm^{-2} $\pm 25\,\%$ (Boersma et al., 2011). This evaluation takes into account the slant column precision, between 0.7 and 1.1×10^{15} molecules cm^{-2} (Boersma et al., 2007; Bucsela et al., 2006), and the uncertainty of tropospheric NO_2 AMF $10-40\,\%$ (depending on the impact of different parameters) (Boersma et al., 2007). Comparisons with in situ measurements from aircraft, ground-based observations from Multi-Axis Differential Optical Absorption Spectroscopy (MAX-DOAS) and Pandora instruments has revealed that OMI tropospheric NO_2 retrievals generally agree within $\pm 20\,\%$ (Lamsal et al., 2014). Several studies that investigated the accuracy of the DOMINO products over rural and urban areas in Russia, Asia, and Indonesia, by using different long-term network observations based on MAX-DOAS (Shaiganfar et al., 2011; Ma et al., 2013; Kanaya et al., 2014), found a negative bias between 26 and 50 % in urban and very polluted areas and when the Aerosol Optical Thickness (AOT) is high. These underestimations have been recently confirmed over Wuxi city, an area with high pollution adjoining Shanghai (Wang et al., 2015b). These low biases could be partially attributed to the inhomogeneity of NO_2 at the spatial scale of OMI observation, and incomplete accounting of NO_2 near the surface. However, the possible additional effects caused by aerosols cannot be ignored. Over industrial regions with comparable photochemical regimes, NO_2 and aerosol concentrations are very well correlated showing similar anthropogenic sources between aerosols and short-lived trace gases (Veefkind et al., 2011).

The current version of the DOMINO algorithm does not explicitly account for the aerosol effects on the tropospheric NO_2 AMF. Similarly, these effects are not explicitly considered in most of the other UV–Vis (ultraviolet–visible) satellite measurements (Valks et al., 2011). Martin et al. (2003) retrieved tropospheric NO_2 columns from the Global Ozone Monitoring Experiment (GOME) instrument by accounting for spatial and temporal variability of aerosols from monthly mean fields of aerosol mass concentration over 1 year simulated by the Global Ozone Chemistry Aerosol Radiation and Transport (GOCART) model. Aerosols affect the top-of-atmosphere (TOA) radiances in the visible and O_2-O_2 spectral bands (Boersma et al., 2011; Leitão et al., 2010) and the light path distribution – i.e. the distribution of distances travelled by photons in the atmosphere before leaving the atmosphere. Since the impacts of aerosols on the computation of tropospheric NO_2 AMF is a function of aerosol properties (Martin et al., 2003), NO_2, and aerosol vertical distribution (Leitão et al., 2010; Bousserez , 2014), a proper characterization of aerosols' impact on the retrieval is then needed to accurately quantify trace gas amounts from satellite observations. The OMI cloud algorithm (Acarreta et al., 2004) derives the cloud fraction and cloud pressure from the O_2-O_2 absorption in the spectral window between 460 and 490 nm. This cloud retrieval algorithm is applied both to cloudy and cloud-free scenes with aerosols. In other words, aerosols are treated as clouds. The correction for the aerosol impact cannot be simply separated from the effects of clouds and, if a cloud retrieval scheme is applied, it will account for a large part of the aerosol effect by retrieving modified cloud fraction and pressure (Boersma et al., 2004, 2011). Wang et al. (2015a) show that OMI cloud parameters are indeed perturbed in the presence of aerosols, by comparing with classified sky conditions using MAX-DOAS observations. Therefore, the cloud retrievals apply an implicit correction of aerosol presence in the computation of the tropospheric NO_2. Recent studies reprocessed the OMI tropospheric NO_2 product, explicitly taking into account aerosols instead of effective cloud retrievals, either by considering model outputs or observations (Lin et al., 2014, 2015; Kuhlmann et al., 2015; Castellanos et al., 2015). These studies were performed over

urban areas in China or biomass-burning events in South America. Resulting changes mostly occurred in the case of high aerosol pollution (AOT > 0.8) with increased or decreased tropospheric NO_2 VCDs depending on the geophysical conditions and aerosol properties. All these studies considered the magnitude of the explicit aerosol correction on the computation of tropospheric NO_2 AMFs and highlighted that aerosol properties and distribution and OMI cloud retrievals are connected. Nonetheless, there is still not a comprehensive understanding of the interplay between aerosol effects on the observations and the associated response of the operational OMI cloud retrieval algorithm. Moreover, the dependence of the retrieved cloud parameters and the associated implicit aerosol correction to the geophysical conditions and the aerosol properties and distribution are not clear. The need to further investigate and understand the interplay between all these variables have been highlighted in different studies (Leitão et al., 2010; Lin et al., 2014). This has recently been emphasized in Castellanos et al. (2015) for the analyses of the implicit aerosol corrections in the case of biomass-burning aerosols.

This paper aims to analyse how aerosols affect the current operational OMI cloud products and the derived tropospheric NO_2 AMFs. For that purpose, this study uses a model vs. observation approach focused on large industrialized areas in China. This work focuses on cloud-free scenes but dominated by aerosol pollution. The paper starts with a description of the expected aerosol net effects on the tropospheric NO_2 AMFs, based on simulations in Sect. 2. The importance of aerosols and NO_2 vertical profiles is highlighted. In Sect. 3, the OMI DOMINO v2 and collocated MODIS (Moderate Resolution Imaging Spectroradiometer) aerosol products are compared over a large industrial area in China. This provides insight into the behaviour of OMI cloud fraction and pressure, and tropospheric NO_2 AMFs in the presence of aerosols. We then evaluate the response of the DOAS O_2-O_2 cloud algorithm on aerosol cases, as achieved by the operational OMI algorithm. The interplay between aerosol effects and the DOAS O_2-O_2 cloud retrieval can be characterized. Finally, in Sect. 4, we show how an implicit aerosol correction is applied in the OMI retrieval chain through the Lambertian cloud model and evaluate its accuracy by comparing it to the explicit aerosol corrections simulated in Sect. 2.

2 Impact of aerosols on the tropospheric NO_2 AMF

2.1 Computation of the tropospheric NO_2 AMF

A two-step approach is used to determine the NO_2 VCD. First, the DOAS method (Platt and Stutz, 2008), based on the basic principle of absorption spectroscopy and the Beer–Lambert law, is applied to the measured spectra within 405–465 nm in order to derive a NO_2 Slant Column Density (SCD). This column gives the number of NO_2 molecules per cm^2, integrated along the average light path. Then, the NO_2 SCD is converted into NO_2 VCD. This can be done by application of the AMF calculated with a radiative transfer model. Note that an intermediate step is to remove the stratospheric part in the NO_2 SCD part in order to derive the tropospheric SCD component. In the DOMINO product the stratospheric SCD is derived from measurements over remote regions that are assimilated into a transport–chemistry model for the stratosphere (Boersma et al., 2011). The AMF A is defined as the ratio of the atmospheric SCD and VCD (Boersma et al., 2011):

$$A(\Psi) = N^{\mathrm{s}}(\Psi)/N^{\mathrm{v}}, \tag{1}$$

where N^{s} is the NO_2 SCD and N^{v} is the NO_2 VCD. The computation of $A(\Psi)$ requires accurate knowledge concerning all the parameters affecting the optical properties of the atmosphere and then impacting the length of the average light path followed by the backscattered sunlight. The list of variables describing these conditions is summarized by Ψ and is detailed in Table 1.

The concept of altitude-resolved AMF was introduced by Wagner et al. (2007), Rozanov et al. (2010), and Richter et al. (2011). Also named block air mass factor or BAMF in other studies, it makes it possible to generalize this definition by computing the AMF variable at discrete atmospheric layers, as

$$a(p^*) = \left.\frac{\Delta N^s(\Psi)}{\Delta N^v}\right|_{\Delta n(p=p^*)}, \tag{2}$$

which describes the altitude dependence of A. The BAMF gives the change in the NO_2 SCD for a change in the vertical column density at one atmospheric layer p (Wagner et al., 2007; Platt and Stutz, 2008; Rozanov et al., 2010; Richter et al., 2011). The a is the altitude-resolved AMF at atmospheric pressure p. The $\Delta n(p = p^*)$ refers to a change in the trace gas profile n at pressure level p^*. ΔN^{v} and ΔN^{s} denote the resulting changes in VCD and SCD respectively. Currently only cloud parameters (and no aerosol parameters) are considered when computing $a(p)$ in the DOMINO product: cloud (radiance) fraction and cloud pressure. A is then computed by weighting $a(p)$ with the atmospheric vertical distribution of the trace gas profile:

$$A = \frac{\int_{p_0}^{p_{\mathrm{top}}} a(p)\cdot n(p)\,\mathrm{d}p}{\int_{p_0}^{p_{\mathrm{top}}} n(p)\,\mathrm{d}p}, \tag{3}$$

where $n(p)$ is the vertical distribution of trace gas density, p_{top} is the pressure at the top of the atmosphere, and p_0 is the surface pressure. In this paper, we define A^{tr} as tropospheric NO_2 AMF, which can be calculated from Eq. (3) by integrating a vertical profile $n(p)$ up to tropopause pressure.

Table 1. List of the physical variables (Ψ) required for the computation of the tropospheric NO_2 AMF, through the altitude-resolved AMF $a(p^*)$. For each of these variables, an indication about its degree of certainty is given.

Ψ		Degree of certainty
SZA (θ_0)		High
VZA (θ)		High
Relative azimuth angle ($\phi - \phi_0$)		High
Wavelength		High
Surface pressure		High
Surface albedo		Moderate
Vertical temperature profile		Moderate
Vertical pressure profile		Moderate
Clouds[a]:	Cloud (radiance) fraction	Moderate to low
	Cloud pressure	Moderate to low
Aerosols[b]:	AOT	Low
	Altitude	Low
Vertical NO_2 profile[c]		Low

[a] Boersma et al. (2007) evaluated that an uncertainty of 0.05 on the cloud fraction and 60 hPa on the cloud pressure respectively contribute up to 30 and 15 % to the (relative) tropospheric NO_2 AMF. While inter-comparison studies show relative good agreements for the OMI cloud fractions (Stammes et al., 2008; Sneep et al., 2008) over cloudy scenes, the retrievals can be affected by aerosols. Thus, the degree of certainty is here evaluated between low (clear and cloudy scenes) and moderate (cloudy scenes). See Sect. 3 for further details.
[b] Section 2 shows that the AOT and aerosol altitude are the key parameters when computing the tropospheric NO_2 AMF. Aerosols impact several parameters (e.g. surface albedo, cloud) in addition to the tropospheric NO_2 AMF.
[c] Maasakers et al. (2013) and Lamsal et al. (2014) showed that using the high-resolution a priori NO_2 profiles impacts the OMI tropospheric NO_2 columns between −43 and 22 %. Aircraft and in situ measurements reveal that NO_2 profile shapes exhibit considerable day-to-day variation, such that the use of a monthly mean profile can cause significant errors in individual retrievals.

The ratio of the altitude-resolved AMF $a(p)$ to the total AMF A (deduced from the NO_2 shape profile) gives the averaging kernel, i.e. the sensitivity of the satellite measurement to each atmospheric layer (Eskes et al., 2003; Richter et al., 2011). Therefore, A^{tr} gives an indication of the sensitivity of the satellite measurement to the amount of NO_2 in the lowest atmospheric layers. Assuming an identical shape of the vertical NO_2 profile, a larger A^{tr} value expresses a higher sensitivity of the measurement while a reduced A^{tr} value indicates a decreased sensitivity. Indeed, in those cases, a change in A^{tr} is directly associated with a change of $a(p)$ at the atmospheric levels where the trace gas is present. The $a(p)$ is in theory spectrally dependent, but the spectral dependence in the case of tropospheric NO_2 retrieval is very small. The reference wavelength considered in this paper is 439 nm (Boersma et al., 2011).

Note that in the case of real OMI tropospheric NO_2 retrievals, a temperature correction should be applied on the SCD. Since the temperature of the NO_2 absorption cross-section is assumed to be fixed at 221 K, a correction term is thus implemented in the computation of A such that it represents the ratio of the NO_2 SCD derived with a NO_2 cross-section at the real temperature T to the column derived at 221 K. European Centre for Medium-Range Weather Forecasts (ECMWF) temperature fields are used for this correction (Boersma et al., 2004, 2011).

2.2 Qualitative description of aerosol optical effects

Similarly to cloud particles, scattering and absorbing effects induced by the presence of aerosol particles affect the total radiance observed by the satellite sensor and the light path distribution of detected photons. The presence of aerosols leads in general to higher radiance levels captured by the satellite sensor. This increase has a spectral variability depending on the aerosol properties. Its magnitude is however smaller in cases of a very bright surface and absorbing aerosols. The change of light path distribution has consequences on the sensitivity of the remote sensing measurement to the tropospheric NO_2 amount. This sensitivity can be either increased or decreased. Qualitatively, one can distinguish two effects that aerosols/clouds can have on the NO_2 absorption signal at the TOA (Leitão et al., 2010):

- Shielding effect: decreased sensitivity within and below the aerosol/cloud layers. The fraction of all detected photons coming from the top of the atmosphere that reaches the lowest part of the atmosphere (below the aerosol/cloud layer) is reduced compared to a cloud- or aerosol-free scene.

- Enhancement (albedo) effect: increased sensitivity within and above the aerosol/cloud layers. The fraction of all detected photons that sample the higher part of the atmosphere (above the aerosol/cloud layer) is in-

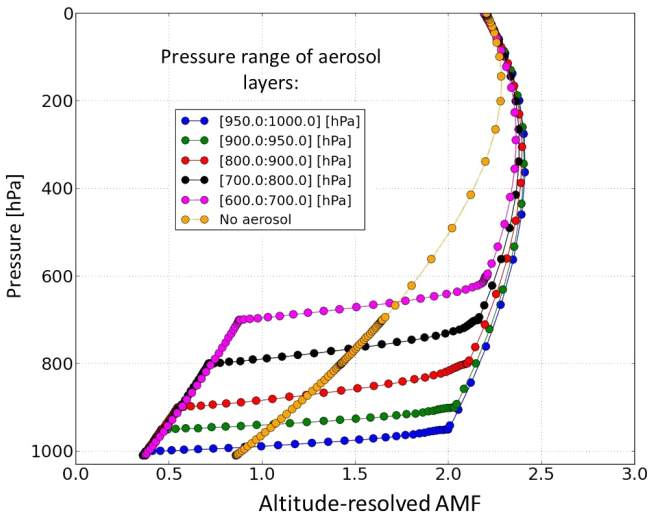

Figure 1. Altitude-resolved AMF at 439 nm as computed by DISAMAR for surface albedo = 0.05, SZA = 25°, VZA = 25°. Computations are done without and with aerosols at different layers. Aerosols are specified with AOT = 1, SSA = 0.95, Ångström coefficient = 1.5 and asymmetry parameter 0.7.

creased, compared to a cloud- or aerosol-free scene, because more photons are scattered back towards the satellite.

Figure 1 depicts an example of vertical distribution of $a(p)$ for a cloud-free observation at 439 nm. With and without aerosols, $a(p)$ values generally decrease close to the surface. Both shielding and enhancement effects can be seen relative to the line for $\tau = 0$. The overall impact of aerosols on a measurement thus depends on the relative importance of the above-mentioned effects, which mainly results from the combination of aerosol optical properties (Martin et al., 2003), amounts, surface reflectance and vertical distribution of the particles, and the NO_2 gas. The geometry parameters like θ_0 (solar zenith angle or SZA) and θ (viewing zenith angle or VZA), and scattering angle (i.e. aerosol phase function) have an impact also as they modify the length of the light path.

2.3 Quantitative description of the impact of aerosols properties, their vertical distribution, and NO_2 profile

2.3.1 Methodology

This section studies the direct effects of aerosols on the computation A^{tr} without consideration of the O_2-O_2 cloud retrieval. This study uses the Determining Instrument Specifications and Analyzing Methods for Atmospheric Retrieval (DISAMAR) software developed at Koninklijk Nederlands Meteorologisch Instituut (KNMI) (de Haan, 2011). This software package includes a radiative transfer model and can apply different retrieval methods, such as direct fitting (within an optimal estimation framework) and DOAS. The radiative transfer model is based on the Doubling Adding KNMI (DAK) model (de Haan et al., 1987; Stammes et al., 2001) and thus computes the reflectance and transmittance in the atmosphere using the adding/doubling method. This method calculates the internal radiation field in the atmosphere at levels to be specified by the user and takes into account Rayleigh scattering, trace gas absorption, and aerosol and cloud scattering. Scattering by aerosols is simulated with a Henyey–Greenstein scattering phase function $\Phi(\cos\Theta)$ (Hovenier and Hage, 1989):

$$\Phi(\cos\Theta) = \frac{1-g^2}{(1+g^2-2g\cos\Theta)^{3/2}}, \quad (4)$$

where Θ is the scattering angle, and $g = \langle\cos\Theta\rangle$ is the asymmetry parameter. In a standard case, an asymmetry parameter of $g = 0.7$ is used. Thus, in DISAMAR, the Ångström exponent α gives the spectral dependence of the AOT τ. In DISAMAR, $a(p)$ is analytically determined, based on the weighting functions of the reflectances (i.e. derivatives of the reflectances to absorption cross-section and trace gas density). Indeed, $a(p)$ for an atmospheric layer can be identified as the Jacobian of the forward model $\partial F/\partial n$. This term is independent of the tracer distribution for optically thin absorbers. This methodology is conceptually equivalent to the approach discussed in Sect. 2.1.

The Henyey–Greenstein phase function is quite commonly used in the DOAS community for tropospheric NO_2 retrievals (Vlemmix et al., 2010; Castellanos et al., 2015) with explicit aerosol corrections. With an asymmetry parameter of $g = 0.7$, the Henyey–Greenstein function is known to reasonably well reproduce the Mie function. Thus, it can be used for the AMF calculation (Spada et al., 2006; Wagner et al., 2007, and P. Stammes, personal communication, 2015). Castellanos et al. (2015) found that decreasing g from 0.7 to 0.6 in DISAMAR impacts less than 5 % the tropospheric NO_2 AMF for AOT lower than 0.5. For larger AOT values, the impacts are almost negligible. It is noted that, for AOT retrievals, more realistic assumptions of the phase function should be used. However, this is not the case for an aerosol correction.

The simulations in this section are done with α of 1.5 for fine particles and 0.5 for coarse particles, asymmetry parameter 0.7 and Single Scattering Albedo (SSA) $\omega_0 = 0.95$ and 0.9 respectively, assuming different altitudes, surface albedos 0.05 and 0.07 (surface reflectance is assumed Lambertian), SZA $\theta_0 = 25°$ and VZA $\theta = 25°$. The ω_0 and τ values are considered at the reference wavelength of 550 nm.The NO_2 profiles are taken from a model run where atmospheric chemistry and transport model Tracer Model 5 (TM5) has been integrated into the global climate model EC-Earth version 2.4 (van Noije et al., 2014). We defined the tropospheric AMF aerosol factor $f(\tau)$ as the ratio of the AMF with $(A^{\mathrm{tr}}(\tau))$ and

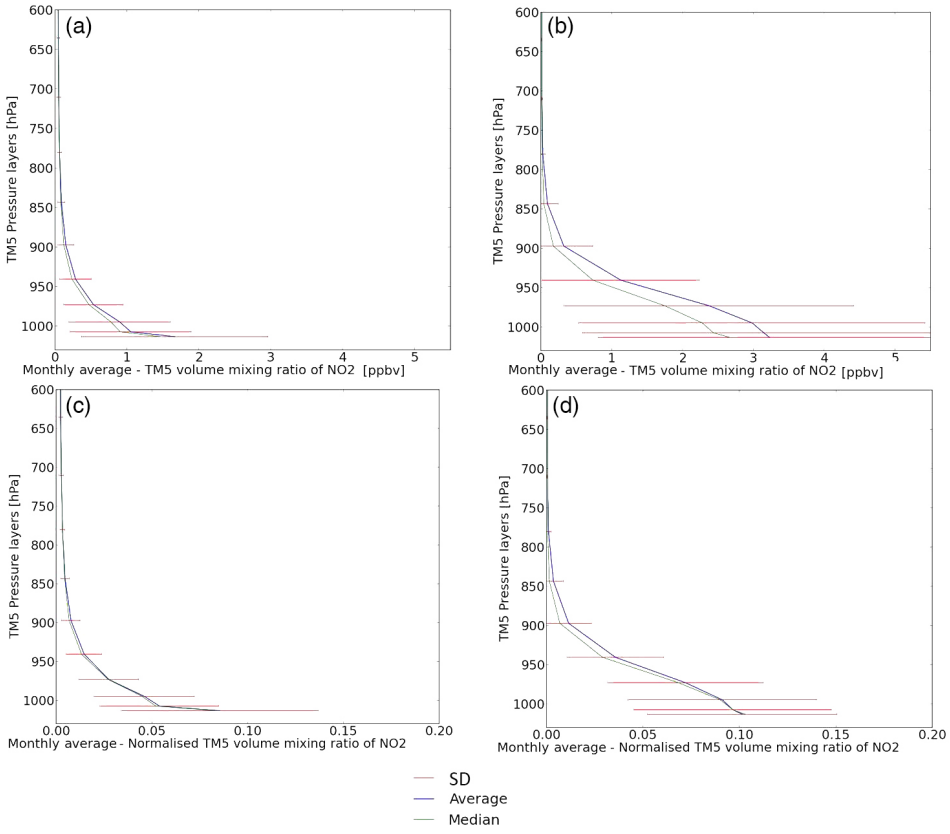

Figure 2. Monthly average NO_2 vertical profiles, zoomed in the troposphere, at 12:00 from TM5 simulations, 2006, East China (van Noije et al., 2014). **(a)** VMR NO_2 profile in July, **(b)** VMR NO_2 profile in January, **(c)** normalized NO_2 profile in July, **(d)** normalized NO_2 profile in January. Normalizations are done by dividing the VMR of each atmospheric layer to the integrated VMR profiles along the vertical atmospheric layers in the complete atmosphere, troposphere + stratosphere. SD here is the standard deviation.

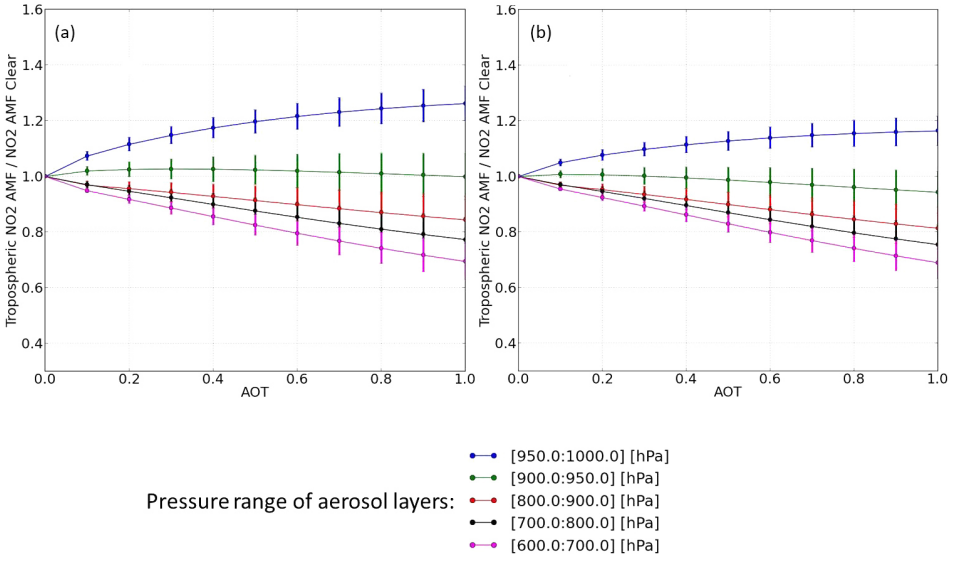

Figure 3. Ratio (f) of AMFs at 439 nm (see Eq. 5) as a function of AOT and aerosol layer altitude for surface albedo = 0.05 **(a)** and 0.07 **(b)**. The f is determined for all the NO_2 vertical profiles from TM5 simulations over East China, July 2006 (see Fig. 1), SZA = 25°, VZA = 25°, aerosol Ångström coefficient = 1.5, SSA = 0.95, and asymmetry parameter = 0.7 for the Henyey–Greenstein phase function. The curves connect the average values per AOT bin and the error bars represent the standard deviation of f computed for all the individual TM5 NO_2 profiles over this period and this region.

without aerosols present ($A^{tr}(\tau = 0)$).

$$f(\tau) = \frac{A^{tr}(\tau)}{A^{tr}(\tau = 0)}. \quad (5)$$

The f can be interpreted as the factor by which the tropospheric NO_2 AMF of a clear scene should be adjusted to represent aerosol effects. In practice, such a factor cannot accurately be determined as not all required information, associated with instantaneous individual measurement, are available. Similarly to the DOMINO product, A^{tr} is computed at 439 nm.

2.3.2 Results

Figure 3 is an example of the computations following Eq. (5) based on all the individual NO_2 profiles generated by the TM5 model for the month of July 2006 at 12:00 (close to the OMI local observation time) over the region of East China (lat. 30–40°, long. 110–130°) (see Fig. 1). The error bars in Figs. 3–5 represent the variability in f due to the variability of the TM5 NO_2 profiles over this region during the month of July. The curves in these figures connect the average values of f per AOT bin.

Figure 3 demonstrates that f lies in the range between 0.7 and 1.3. The total effect of aerosols (shielding or enhancement) strongly depends on the location of the particles in the atmospheric layers, and results from the computed $a(p)$ depicted in Fig. 2. Scattering of aerosols enhances the tropospheric NO_2 A up to 30 % for $\tau = 1.0$ when they are located within or below the NO_2 bulk (between the surface and 900 hPa). When a given amount is lifted to higher altitudes, aerosols thus apply a shielding effect (i.e. reduced sensitivity to the tropospheric NO_2 amount) up to 30 %. The variability of the NO_2 vertical distribution impacts the magnitude of these effects, around 10 % for $\tau = 1$.

In addition to the vertical distribution of the aerosol particles, the shape of the vertical NO_2 profile also significantly affects the magnitude of f. In winter (e.g. January in Fig. 1), such profile shows higher absolute values of concentrations near the surface with a higher variability. Moreover, the profile shape (obtained after normalization to the integrated vertical profile along the atmospheric layers) depicts a small difference with a higher dynamic between the surface and the atmosphere layer at 900 hPa. Figure 4a shows amplified enhancement effects (up to 40 % for aerosols between the surface and 950 hPa) and amplified shielding effects (up to 45 % for aerosols at very high altitude, between 600 and 700 hPa). The transition between a net shielding or enhancement effect is also closer to the surface compared to summer (close to 950 hPa) as the aerosols are well mixed with the tropospheric NO_2 bulk only below 950 hPa. The variability of the NO_2 profile, mostly in the tropospheric layers, have a larger impact in January, where the error bars indicate a variability of around 20 % for $\tau = 1.0$. The altitudes of tropospheric NO_2 and aerosols, and so the relative altitude between both, are thus the key drivers of f.

Other parameters also contribute to the magnitude of this factor:

- An increase of surface albedo (see Fig. 3b), from 0.05 to 0.07, reduces the enhancement effect by 10 % and enhances the shielding effect by less than 5 % for $\tau = 1.0$.
- The size of particles specified through α has little impact on the factor (see Fig. 5a). Decreasing α from 1.5 (fine particles) to 0.5 (coarse particles) reduces the shielding and enhancement effects by between 2 and 5 % for $\tau = 1.0$.
- A change of ω_0 from 0.95 to 0.9 (see Fig. 5b) leads to a reduction of the enhancement effect by 10 % (when aerosols are located below or well mixed with the tropospheric NO_2 bulk). The shielding effect is increased by 5 %.
- The increase of θ_0 from 25 to 50° (typically Winter average over China), increases the shielding effects by 10 % for $\tau = 1.0$ (assuming NO_2 profiles in January). Moreover, the enhancement effect increases between 5 and 10 % for τ between 0.3 and 0.7.
- The monthly variability of the NO_2 profiles increases the variability of f, expressed by the error bars in Fig. 3, when aerosols are located close to the surface between 900 and 1000 hPa. This is a direct consequence of the enhancement effect induced by aerosol particles that increase the sensitivity to the NO_2 in the lower part of the atmosphere.

Our results are consistent with previous findings by Leitão et al. (2010) and Bousserez (2014) who used different theoretical NO_2 and aerosol vertical distributions and optical properties. In particular, our present exercise considered various NO_2 profiles, as given by the TM5 model, representative of 2 distinctive months (July and January), and thus of 2 typical seasons, over urban areas in China. Moreover, the monthly variability of these profiles, and thus their impacts on the tropospheric NO_2 AMF variability, are investigated as a function of aerosol properties and vertical profile giving then complementary insights about explicit aerosol effects. These results are also in line with the work of Martin et al. (2003) where strongly absorbing aerosols reduced the AMF by 40 % (over biomass-burning regions) while scattering sulfate and organic aerosols increased the AMF by 5–10 %.

3 Interplay between aerosols and the OMI O_2-O_2 cloud retrievals

This section explains the perturbations induced by the aerosol particles on the retrieval of cloud fraction and cloud

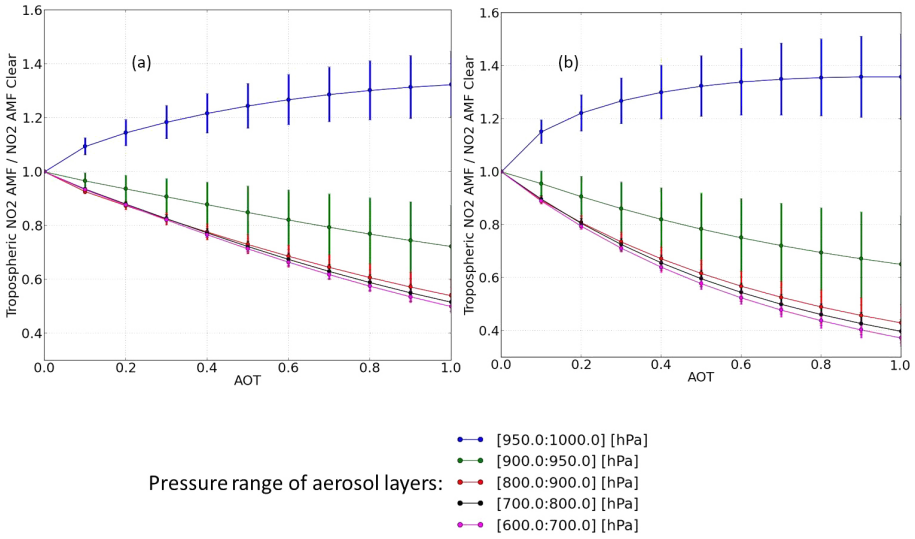

Figure 4. (a) Similar to Fig. 3a, but with NO_2 profiles for January. **(b)** Similar to Fig. 4a, but with SZA = 50°.

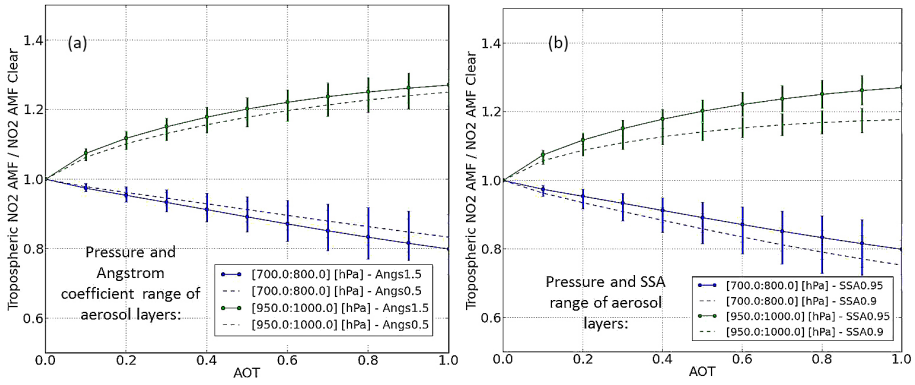

Figure 5. Similar to Fig. 3, but with only two different atmospheric aerosol layers: **(a)** two Ångström coefficient values: 1.5 (fine particles) and 0.5 (coarse particles); **(b)** two SSA values: 0.95 and 0.9.

pressure based on the OMI O_2-O_2 spectral band. This section is structured as follows: first the OMI DOMINO product is analysed in comparison with the MODIS Aqua aerosol product. Then, the OMI DOAS cloud O_2-O_2 retrieval chain is analysed with simulated aerosol cases.

3.1 Comparison of OMI DOMINO-v2 with MODIS Aqua aerosol product

MODIS on-board EOS-Aqua observes the Earth's atmosphere approximately 15 min prior to OMI on-board EOS-Aura. The aerosol effects on the current OMI tropospheric NO_2 retrievals are investigated by comparing collocated OMI DOMINO with MODIS Aqua Level 2 (L2) aerosol products over large industrialized areas in China. Statistics are computed over 3 years (2005–2007) and 2 seasons: summer (June, July and August) and winter (December, January and February). MODIS L2 aerosol products have a spatial resolution of 10 km × 10 km, therefore close to the OMI spatial resolution (13 km × 24 km at nadir). The OMI and MODIS data are paired on a pixel-by-pixel basis if the distance between pixel centres is less than 5 km and if both observations are acquired within 15 min. Observations with a cloud fraction (OMI and MODIS) higher than 0.1 are filtered out. This threshold is applied to both OMI and MODIS, although the parameters are not identical. Applying such a threshold on the observations increases the probability of identifying cloud-free scenes. Moreover, the availability of the MODIS aerosol product is a good confirmation of the identification of cloud-free scenes as MODIS Aqua AOTs τ are exclusively retrieved for cloud-free situations (Remer et al., 2008). However, it is well recognized, according to the analyses in the next section, that cloud-free observations with large presence of aerosols are filtered out as well. Tests were performed with higher cloud fraction thresholds (0.2 and 0.3) showing no statistically significant changes in the results described below.

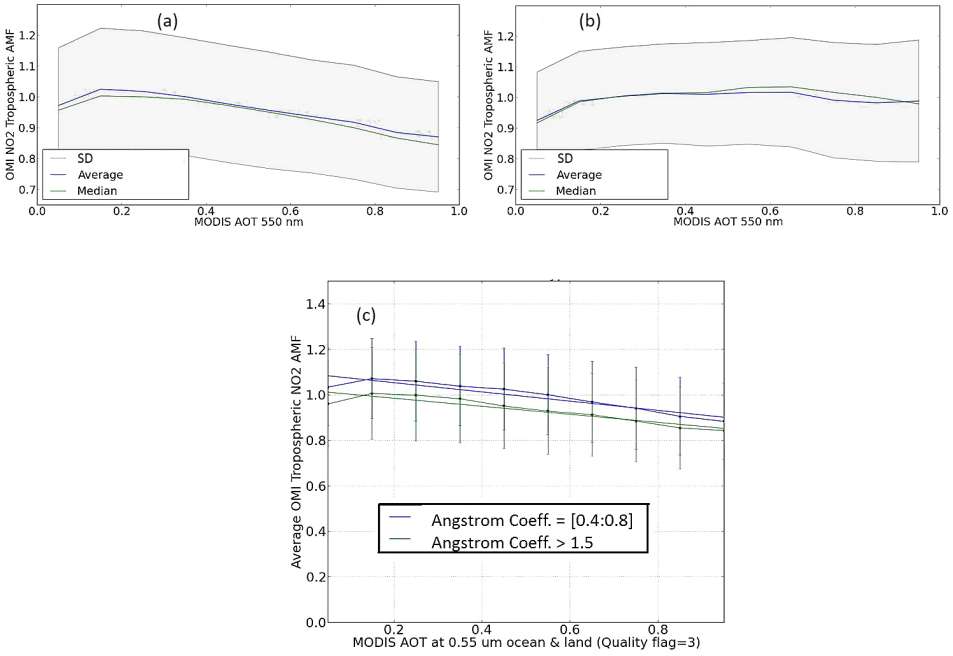

Figure 6. Tropospheric NO_2 AMFs from the OMI DOMINO v2 plotted against MODIS Aqua AOT. Statistics are computed over 3 years (2005, 2006, 2007) and following the methodology described in Sect. 3: **(a)** summer (June, July, August), **(b)** winter (December, January, February), over East China, **(c)** summer, distinction between two ranges of MODIS Aqua aerosol Ångström coefficient. SD here is the standard deviation.

The tropospheric NO_2 AMF (A) that is extracted from the OMI DOMINO database shows a decreasing trend with increasing τ in summer (see Fig. 6a). This decrease is on average 5 % for MODIS $\tau = 1$, with a variability of 20 %. A small local positive trend (around 5 %) is however noticed for $\tau = 0$–0.2. In contrast, in winter, there is on average no modification of the tropospheric NO_2 AMF A with increasing τ (see Fig. 6b). By making use of the Ångström coefficient α available in MODIS AQUA data (see Fig. 6c), it is found that A is larger for coarse particles than for fine particles (differences of 10 %). Such statistics also include spatial variability in τ and NO_2, so that the apparent correlations between them may be affected by other spatial factors like surface albedo or elevation.

Figures 7–9 depict the impact of aerosols on the OMI O_2-O_2 cloud fraction and pressure. Under aerosol presence and no cloud contamination in the OMI measurement, the OMI cloud fraction shows a clear linear relation with respect to τ. On average, values increase from 0.01 to 0.07 with a variability of 30 % for $\tau = 1$. The magnitude of this increase depends on the surface albedo (Kleipool et al., 2008) and MODIS Aqua aerosol properties:

– The increase of cloud fraction with increasing AOT is higher over dark surfaces and lower over bright surfaces (average differences of 0.03 for $\tau = 1$, between OMI surface albedos of 0.04 and 0.08; see Fig. 8). As analysed in detail in Sect. 3.3.1., this is a direct consequence of the aerosol effects on the continuum reflectance. The attenuation of surface reflectance by particles is stronger over bright surfaces than over dark surfaces. Over a brighter surface, aerosols play the role of a surface layer with a higher albedo as they increase the scene brightness. As a consequence, the retrieved effective cloud fraction value is higher.

– Cloud fraction values are higher in the presence of small particles (average differences of 0.03 between MODIS Aqua α of [1.5 : 1.8] and [0.4 : 0.8]; see Fig. 9).

The cloud pressure values show a non-linear decrease from approximately 800 to 600 hPa for $\tau = 1$, with a variability of around 100 hPa during summer (see Figs. 8 and 9). However, no decrease is observed during winter. The cloud pressure stays close to the surface (between 900 and 1000 hPa). The retrieved cloud pressure seems to have some sensitivity to the surface and aerosol properties. In particular, it decreases more over dark surfaces (difference of 100 hPa between surface albedo 0.04 and 0.07 for $\tau = 1$) and in the presence of fine particles.

This section follows previous studies (Boersma et al., 2011; Lin et al., 2014; Castellanos et al., 2015) by analysing the OMI cloud and AMF parameters as present in the DOMINO product over scenes dominated by aerosols. It confirms that the cloud parameters respond to the presence of aerosols. The magnitude of this response is not only a function of aerosol properties but also of the atmospheric and sur-

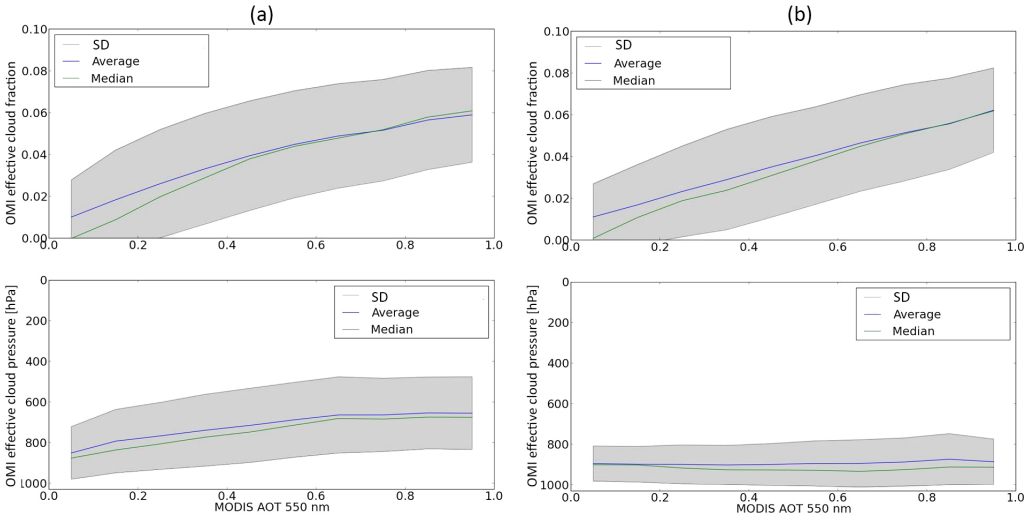

Figure 7. Effective cloud fraction and cloud pressure extracted from OMI DOMINO v2 compared to MODIS Aqua AOT for 2 seasons. Statistics are computed over 3 years (2005, 2006, 2007) and following the methodology described in Sect. 3.1: **(a)** summer (June, July, August), **(b)** winter (December, January, February) over East China. SD here is the standard deviation.

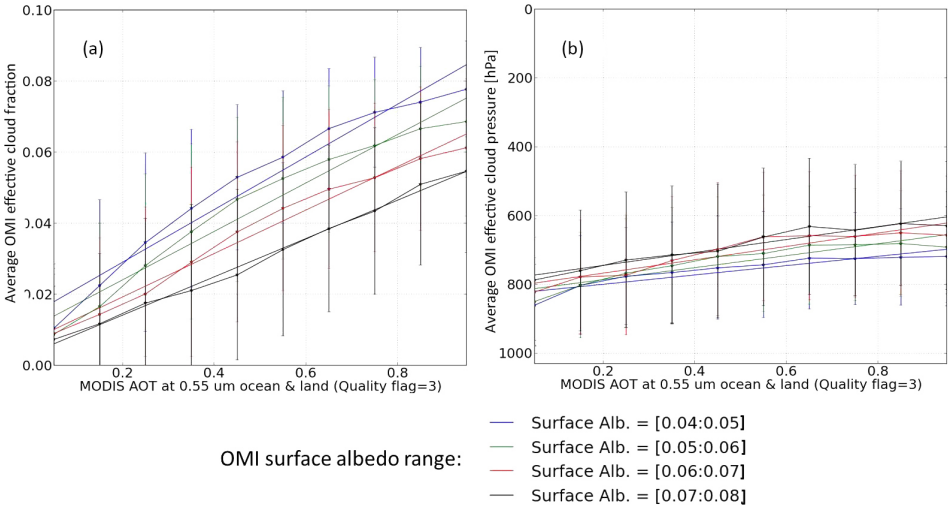

Figure 8. OMI effective cloud parameters extracted from OMI DOMINO v2 compared to MODIS Aqua AOT, as a function of the OMI climatology surface albedo (Kleipool et al., 2008). Statistics are computed over 3 years (2005, 2006, 2007) in summer (June, July, August) over East China (see Sect. 3.1): **(a)** effective cloud fraction, **(b)** effective cloud pressure.

face properties that impact the average light path (e.g. surface albedo). One may conclude that there is an implicit correction for the presence of aerosols in the tropospheric NO_2 retrieval chain since the OMI cloud algorithm cannot distinguish cloud and aerosol particles and retrieve effective cloud parameters. The computation of the tropospheric NO_2 AMF relies on the NO_2 vertical shape profile and aerosol properties (that drive the OMI cloud retrievals). Both parameters have different characteristics depending on the season. As a consequence, the implicit correction seems to show two different behaviours depending on the seasons. On average, this correction applies a shielding effect in summer: i.e. the measurements are assumed to have less sensitivity to tropospheric NO_2 in the presence of aerosols. In winter, this correction on average does not vary with increasing AOT values.

3.2 Qualitative description of the OMI cloud algorithm

3.2.1 Inverse cloud model

In the context of trace gas measurements from space, the purpose of a cloud model is to describe the clouds in a way that reproduces the reflectance spectrum, and thus the distribution of photon paths, within the cloudy scenes. For this purpose, the parameters of such a model are cloud fraction,

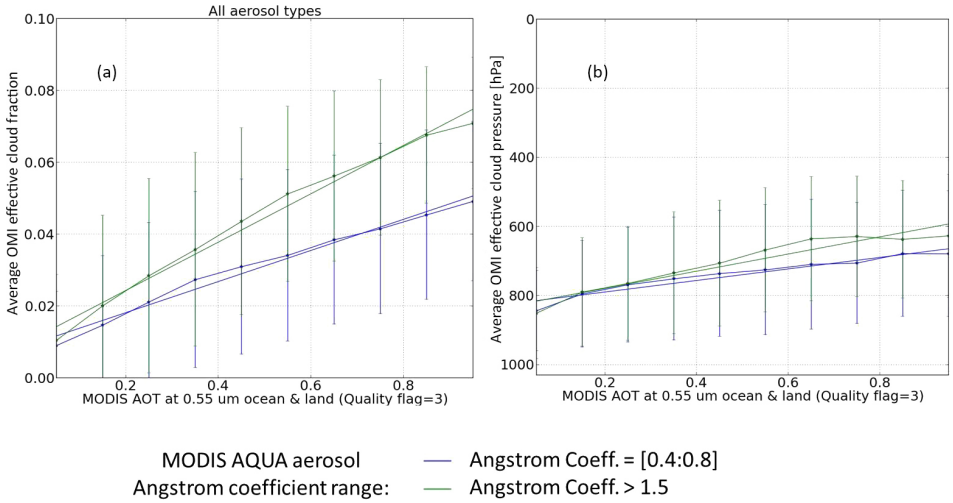

Figure 9. Similar to Fig. 8 but as a function of the MODIS aerosol Ångström coefficient: **(a)** effective cloud fraction, **(b)** effective cloud pressure.

cloud optical thickness, cloud top altitude, and cloud vertical extent. However, instruments like OMI have limited spatial resolution (13 km × 24 km at nadir view) and do not resolve individual clouds. Therefore, cloud fraction and cloud optical thickness cannot be separated. Furthermore, OMI cannot give information on cloud microphysical properties such as cloud phase, cloud particle shape and size, and cloud vertical structure.

Because clouds are a correction step in trace gas retrievals, both the cloud retrieval algorithm and the cloud correction algorithm have to use the same cloud model. As a consequence, a simple model is used in the OMI tropospheric NO_2 retrievals, describing a cloud as a Lambertian reflector with a fixed albedo through which no light is transmitted. The associated effective cloud fraction is thus not a geometric cloud fraction but the radiometrically equivalent cloud fraction which, in combination with the assumed cloud albedo, yields a TOA reflectance that agrees with the observed reflectance. While scattering clouds have two main optical properties in the UV–Vis (namely reflection and transmission – their absorption being negligible), a Lambertian reflector has only reflection properties, determined by the cloud albedo, and no transmission properties. The OMI cloud retrieval algorithm assumes a cloud albedo of 0.8 (Stammes et al., 2008). This value has been found suitable to correct NO_2 and O_3 retrievals for partially cloudy scenes. The missing transmission of optically thin and medium thick clouds in the Lambertian cloud model is compensated for by the cloud-free part of the pixel.

Based on the properties of an opaque Lambertian cloud model, the effective cloud fraction is mainly constrained by the brightness of the cloud and how much a brighter cloud would outshine the observation scene. The effective cloud pressure is mainly constrained by the perturbation of the clouds on the O_2-O_2 collision complex absorption. A cloud located at high altitude shields the O_2-O_2 complexes that are below the cloud. As a consequence, the O_2-O_2 absorption signal, and so the associated slant column density, are attenuated (Acarreta et al., 2004; Stammes et al., 2008; Sneep et al., 2008).

3.2.2 Description of the O_2-O_2 DOAS retrieval algorithm

The OMI cloud retrieval chain (Acarreta et al., 2004) exploits the 460–490 nm absorption band of O_2-O_2, a collision pair of oxygen. The retrieval algorithm is based on the DOAS method and consists of two steps. In the first step, the absorption cross-section spectrum of O_2-O_2 is fitted together with a first-order polynomial to the negative logarithm of the measured reflectance spectrum. The window of the spectral fit is 460–490 nm. This step can be summarized as follows:

$$-\ln(R) = \gamma_1 + \gamma_2 \cdot \lambda + N^{\mathrm{s}}_{\mathrm{O_2-O_2}}(\lambda) \cdot \sigma_{\mathrm{O_2-O_2}} + N^{\mathrm{s}}_{\mathrm{O_3}}(\lambda) \cdot \sigma_{\mathrm{O_3}}, \quad (6)$$

where $\gamma_1 + \gamma_2 \cdot \lambda$ defines the first-order polynomial, $\sigma_{\mathrm{O_2-O_2}}$ is the O_2-O_2 absorption cross-section spectrum (at 253 K), $\sigma_{\mathrm{O_3}}$ is the O_3 absorption cross-section spectrum, $N^{\mathrm{s}}_{\mathrm{O_3}}$ is the O_3 SCD and $N^{\mathrm{s}}_{\mathrm{O_2-O_2}}$ is the O_2-O_2 SCD. The O_3 cross-section spectrum is included because it overlaps with the O_2-O_2 spectrum. The fitted parameters are γ_1, γ_2, $N^{\mathrm{s}}_{\mathrm{O_2-O_2}}$, and $N^{\mathrm{s}}_{\mathrm{O_3}}$. In the absence of absorbers, one may define the continuum reflectance R_{c} at the reference wavelength λ_0:

$$R_{\mathrm{c}} = \exp(-\gamma_1 - \gamma_2 \cdot \lambda_0). \quad (7)$$

The reference wavelength is fixed at the middle of the DOAS fit window at $\lambda_0 = 475$ nm.

In the second step, a Look-Up-Table (LUT) is used to convert the retrieved $N^{s}_{O_2-O_2}$ and R_c into the cloud pressure C_p and cloud fraction C_f. This inversion step requires prior information about surface albedo, surface altitude, and geometry angles (θ_0, θ and the relative azimuth angle $\phi - \phi_0$).

3.3 OMI cloud algorithm applied to aerosol scenes

To test the sensitivity to aerosols, the current version of the OMI DOAS O_2-O_2 algorithm was applied to simulated spectra for scenes dominated by aerosols. The implementation was performed in such a way that it is almost identical to the operational DOMINO chain at KNMI. The effective cloud fraction and cloud pressure parameters are derived following Eqs. (6) and (7) and through linear interpolation in the LUT, assuming thus an opaque Lambertian cloud model as described previously. Reflectance spectra are simulated by including only aerosol particles with the DISAMAR software. No clouds are included in the simulated reflectances. The sensitivity of the retrievals are investigated as a function of surface albedo, aerosol properties (α, ω_0, vertical distribution), θ_0, and θ. Simulated reflectances are noise-free. All the parameters (including surface albedo) are identical in the simulated spectra dominated by aerosols and the retrieval of effective cloud parameters.

3.3.1 Response of the cloud fraction to aerosol scenes

Figure 10a shows that the effective cloud fraction increases with increasing τ in cloud-free scenes up to 0.09 for $\tau = 1.0$ at the wavelength of 550 nm, assuming fine particles ($\alpha = 1.5$), high single scattering albedo ($\omega_0 = 0.95$), $\theta_0 = 25°$ (summer in China), and $\theta = 25°$. Here, aerosols are located between 700 and 800 hPa in the atmosphere (between approximately 2 and 3 km). Similarly to what has been observed in the DOMINO product, the increase of the effective cloud fraction, in the presence of aerosols, is linear and higher with lower surface albedo (i.e. over dark surfaces). In this case, with a surface albedo of 0.07, the effective cloud fraction stays below 0.09 for $\tau = 1.0$ while, with a surface albedo of 0.03, the value is close to 0.1. Such an increase is consistent with the impact of the aerosol particles on the continuum reflectance as a function of τ and surface albedo. For these surface albedos and aerosol properties, the scattering effects of aerosols dominate over their extinction.

Figure 10b and c illustrate that aerosol properties (size and absorption) drive the magnitude of the increase of effective cloud fraction. Notably, low α and ω_0 values have smaller impact on the increase of the effective cloud fractions. This illustrates the reduction of scattering effects of aerosols under these conditions. Indeed, low ω_0 values increase the probability of absorption of the photons and so reduce the scattering within the layers and towards the satellite sensor. Coarse particles reduce also the scattering effects by increasing the probability of forward scattering of the photons towards the top of the atmosphere or towards the surface. With fine particles, the effective cloud fraction varies between 0.06 ($\omega_0 = 0.9$) and more than 0.1 ($\omega_0 = 0.97$) for $\tau = 1.0$.

As a consequence, a higher cloud fraction is understood from the excess TOA reflectance caused by the additional scattering due to aerosols and the impact of the surface reflection. This represents the significant enhanced brightness of the scene (or enhanced scene albedo).

3.3.2 Response of the cloud pressure to aerosol scenes

Figure 11 shows that the retrieved effective cloud pressure decreases with increasing τ (or AOT). This decrease is linked to the O_2-O_2 shielding effect which strongly depends on τ. The O_2-O_2 absorption, below the optically thicker aerosol layer, is reduced since a high amount of particles decreases the fraction of photons reaching the lowest part of the atmosphere and increases the attenuation of the surface reflectance signal. Therefore, the length of the average light path is shortened. At high τ values, the retrieved cloud pressure correlates with the aerosol layer height. Overall, the values are close to or smaller than the mean aerosol layer height which may be caused by the model error (i.e. difference between the cloud model and the aerosol spectral effects). Surprisingly, at small τ values, the mean aerosol layer height has no effect on the retrieved cloud pressure. The retrieved values stay very close to the surface pressure.

The OMI cloud LUT has been intended for representing the cloud spectral effects and not those of thin aerosol layers. Thus, the sampling may be not high enough in the case of low cloud fraction values (i.e. smaller than 0.1). Such values have limited effects on the average light path and the actual designed LUT is not sensitive enough to small changes on the O_2-O_2 absorption (Acarreta et al., 2004). Since low amounts of aerosol have little effect on the O_2-O_2 SCD and the continuum reflectance, the overestimation of the retrieved cloud pressure, in those cases, may be caused by the coarse sampling of the employed LUT. When τ increases, the considered entry in the LUT moves from this undetermined regime to a regime where meaningful cloud pressure value can be interpreted. This can be seen in Fig. 10a–c where the transition between both regimes is located between $\tau = 0.6$ and $\tau = 0.8$, assuming $\theta_0 = 25°$ and $\theta = 25°$. This demonstrates a non-linear behaviour between the cloud pressure retrieval and the AOT. Such behaviour is consistent with the analyses of Boersma et al. (2011), over southern and eastern USA, which show that reduced OMI O_2-O_2 cloud pressure values are observed only with high AOTs. Wang et al. (2015a) found that in general the effective cloud fraction of up to 15 % and cloud top pressure from the surface to 900 hPa from OMI are assigned to the condition of "clear sky with presence of aerosol particles".

The value of τ at which the retrieved cloud pressure starts being sensitive to the aerosol layer height mainly depends

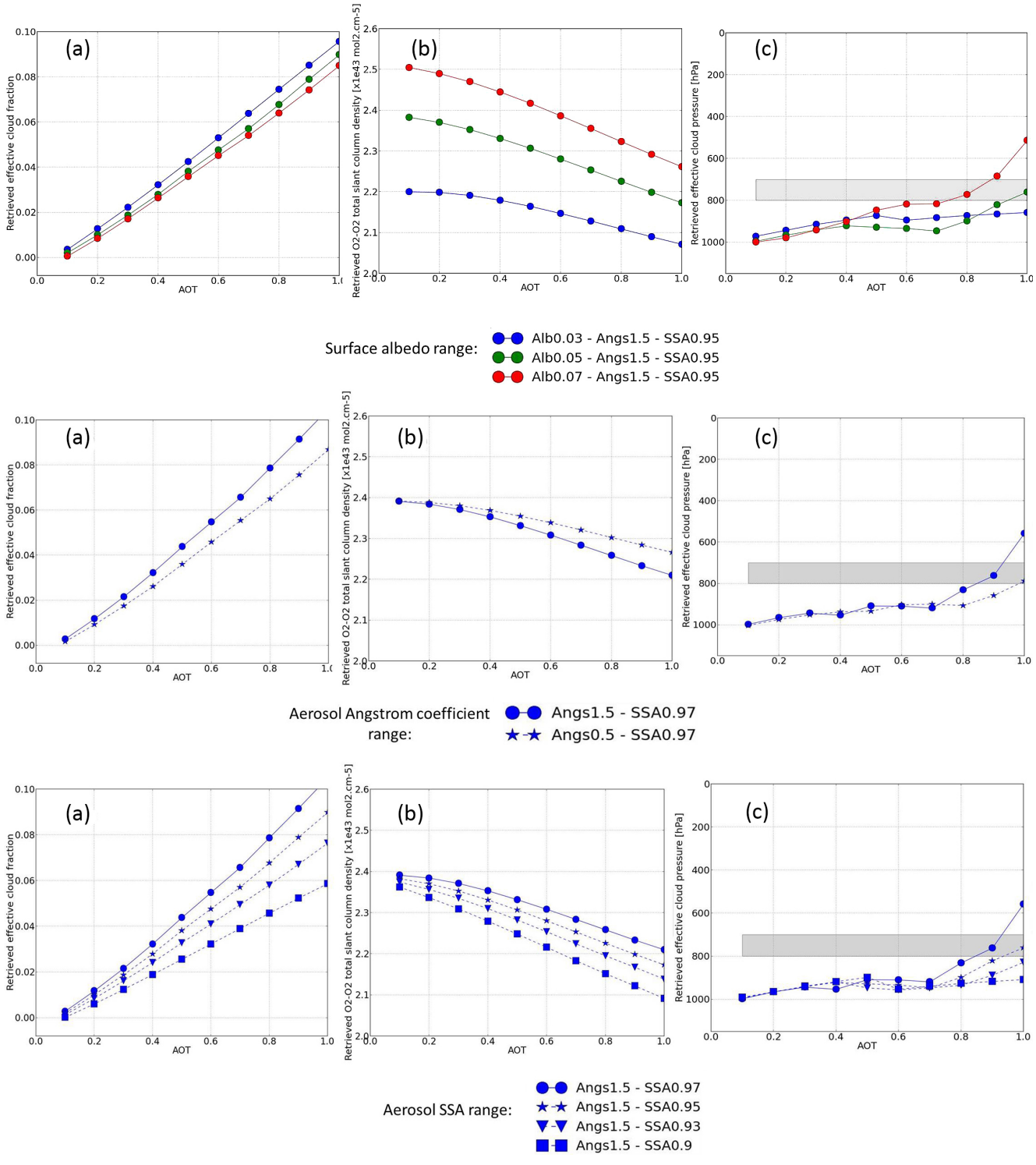

Figure 10. (a) Effective cloud, **(b)** O_2-O_2 total SCD, **(c)** effective cloud pressure (grey colour depicts the location of the simulated aerosol layers). Top panel: Simulated DOAS O_2-O_2 cloud retrieval results, based on noise-free spectra with aerosols, as a function of AOT and surface albedo, assuming an opaque (albedo = 0.8) Lambertian cloud forward model. The results are derived from the following geophysical conditions: average of temperature, H_2O, and NO_2 vertical profiles from TM5 month July (see Fig. 1), O_2 total column = 250 DU, SZA = 25 ("°" for deg), and VZA = 25 ("°" for deg), surface pressure = 1010 hPa. Aerosol properties are SSA = 0.95, Ångström coefficient = 1.5 (fine particles), asymmetry parameter = 0.7, layers located between 700 and 800 hPa. Middle panel: as top panel but the results are depicted as a function of Aerosols AOT and Ångström coefficient. The surface albedo is here constant (0.05). Bottom panel: As top panel but the results are depicted as a function of Aerosols AOT and SSA. The surface albedo is here constant (0.05).

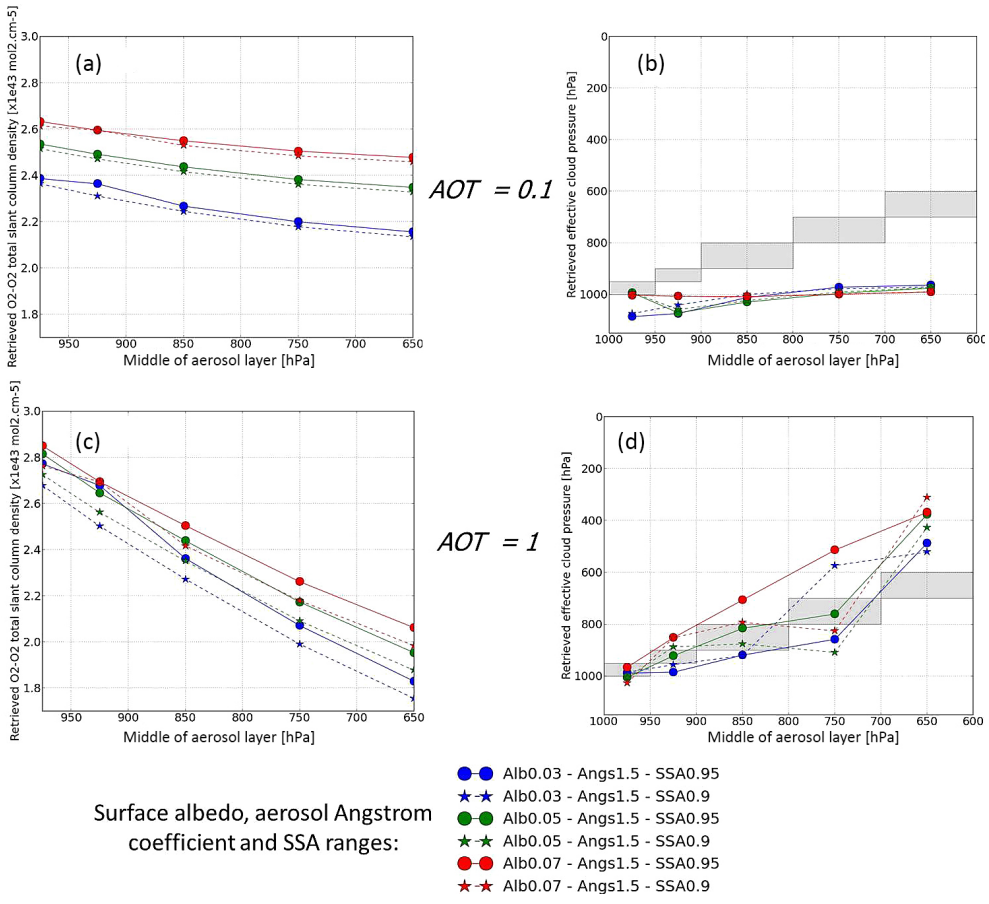

Figure 11. Impact of the location of atmospheric aerosols layers on the simulated DOAS O_2-O_2 cloud retrieval results as a function of AOT and surface albedo. The results are derived from conditions of Fig. 10a: **(a)** O_2-O_2 total SCD for AOT = 0.1, **(b)** effective cloud pressure (grey colour depicts the location of the simulated aerosol layers) for AOT = 0.1, **(c)** O_2-O_2 total SCD for AOT = 1, **(d)** effective cloud pressure for AOT = 1.

on the geometry. Figure 12 shows that for larger θ_0 and θ values (i.e. more than 25°), this transition triggers at smaller τ values (around $\tau = 0.4$). This can be understood as an increased average path length travelled by the photons in the atmosphere and higher retrieved effective cloud fraction values (up to 0.15). Note that change of relative azimuth angle may have similar effects.

The effects of aerosol microphysics properties on the effective cloud pressure retrieval mainly depend on the aerosol amount and the geometry. While smaller α and ω_0 values lead to smaller O_2-O_2 SCDs (see Fig. 10b and c), the associated effective cloud pressure only decreases: for τ well above 1 in the case of small angles ($\theta_0 = 25°$ and $\theta = 25°$); or between $\tau = 0.6$ and $\tau = 1$ in the case of large angles ($\theta_0 = 50°$, or $\theta = 45°$). Finally, cases with high surface albedo show smaller retrieved effective cloud pressure. The brighter the surface, the more the average photon path length is reduced by a thin aerosol layer. This also highlights that a bias on the assumed surface albedo can perturb the effective cloud pressure retrieval in cases of high aerosol amount. For instance, an overestimated surface albedo (because of scattering aerosol affects) can lead to reduced effective cloud pressure.

Based on these simulations and retrievals, we can now largely understand the decrease of the effective cloud pressure in summer over China. Partly, this is a consequence of presence of fine aerosol particles (most of the MODIS Ångström coefficients are beyond 1.5). Moreover, the boundary layer is generally deeper in summer due to convective growth. The high cloud pressures for low τ values are largely a retrieval artifact (as discussed above); the lower cloud pressures for higher τ are probably more realistic, as in the regime of high τ there is more sensitivity to the layer height (Fig. 10). In winter, this transition from almost no sensitivity at low τ to more sensitivity to the layer height at high τ results in an almost flat curve, probably because the boundary layer itself is quite shallow. The variability that is seen in Fig. 7 is related to the different effects of surface reflectance and variable viewing angles.

Table 2. List of values considered for the simulation nodes illustrated in Fig. 13: effective cloud fraction, effective cloud pressure, aerosol optical thickness, and aerosol pressure.

Parameter	List of values
Effective cloud fraction	0., 0.01, 0.02, 0.04, 0.06, 0.08, 0.1, 0.125, 0.15, 0.175, 0.2, 0.25, 0.3, 0.35, 0.4, 0.45, 0.5, 0.55, 0.6, 0.65, 0.7, 0.75, 0.8, 0.95, 1., 1.1, 1.2
Effective cloud pressure [hPa]	1013, 963, 913, 863, 813, 763, 713, 663, 613, 563, 513, 463, 413, 363, 313, 263, 213, 163, 113, 63
Aerosol optical thickness	0., 0.01, 0.02, 0.03, 0.04, 0.05, 0.06, 0.07, 0.08, 0.09, 0.1, 0.15, 0.2, 0.25, 0.3, 0.35, 0.4, 0.45, 0.5, 0.55, 0.6, 0.65, 0.7, 0.75, 0.8, 0.85, 0.9, 0.95, 1., 1.05, 1.25, 1.5, 1.75, 2., 2.25, 2.5, 2.75, 3., 3.25, 3.5, 3.75, 4
Aerosol pressure [hPa]	975, 950, 925, 875, 850, 825, 800, 775, 750, 725, 700, 675, 650 550, 450, 350, 250, 150

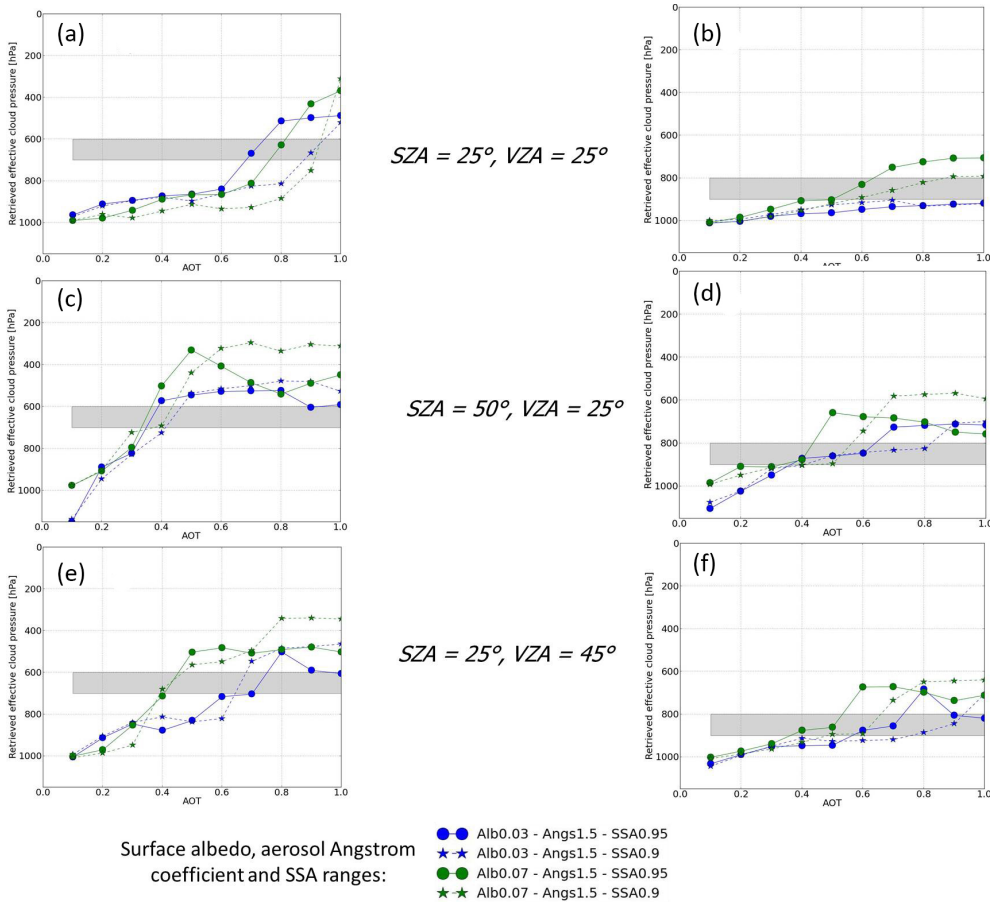

Figure 12. Impact of geometry angles on the effective cloud pressure retrievals as a function of surface albedo, aerosol microproperties, AOT, and location of atmospheric aerosol layers (grey colour depicts the location of the simulated aerosol layers). The same conditions as in Fig. 10a are assumed: **(a)** and **(b)** SZA = 25° and VZA = 25°, **(c)** and **(d)** SZA = 50°, VZA = 25°, **(e)** and **(f)** SZA = 25°, VZA = 45°.

3.4 General inter-comparison of cloud and aerosol impacts on the O_2-O_2 spectral band

The previous analyses clearly show the limitation of the response of the current OMI cloud algorithm, in particular the effective cloud pressure retrieval, due to the not-optimized OMI cloud LUT over clear-sky scenes dominated by aerosol particles. The use of a LUT cannot be avoided since it is required to convert the continuum reflectance and the O_2-O_2 SCD into effective cloud parameters. Since different LUTs

may give different results, the following exercise (summarized in Fig. 13) illustrates in a general way how aerosols and OMI effective cloud retrievals should be connected. O_2-O_2 spectra (from 460 to 490 nm) were simulated containing either an opaque Lambertian cloud (albedo = 0.8) assuming different cloud fraction and pressure values, or box fine and scattering aerosol layers with different AOT and aerosol pressure values (see list of values in Table 2). A very high sampling in the simulation nodes (i.e. cloud fraction, cloud pressure, AOT, and aerosol pressure values) is considered. Then a DOAS fit is achieved as described in Sect. 3.3.2. Finally, a linear interpolation/extrapolation, based on the radial basis function, is performed in order to have a global overview of the variation of the simulation nodes as a function of the DOAS fit variables. The accuracy of the linear interpolation/extrapolation is here ensured thanks to the very high sampling of the simulation nodes.

As expected, Fig. 13 confirms that the effective cloud fraction is primarily constrained by the continuum reflectance, while the O_2-O_2 SCD mainly drives the effective cloud pressure. Similarly, following the previous analyses, AOT mostly impacts the continuum reflectance while the aerosol altitude (or aerosol pressure) mostly results in a change of O_2-O_2 SCD. Furthermore, in the case of low-continuum reflectance (below than 0.2), which corresponds to aerosol cases and low effective cloud fraction, some correlations are observed between both DOAS fit variables.

Therefore, in the case of an ideal O_2-O_2 cloud retrieval (i.e. without the specific limitation of the current employed OMI cloud LUT), the following is expected:

- For a given aerosol altitude value, increasing AOT should result in a larger continuum reflectance and thus increase the effective cloud fraction;
- For a given AOT value, increasing the aerosol altitude (or decreasing pressure) should result in smaller O_2-O_2 SCD and thus decrease the effective cloud pressure;
- Since increasing AOT primarily impacts the continuum reflectance but also simultaneously impacts the O_2-O_2 SCD, retrieved effective cloud pressure could theoretically either increase, decrease or stay constant depending on the aerosol altitude. This demonstrates that the magnitude of the O_2-O_2 shielding effect by aerosols is a combination of aerosol amount and altitude.

The high sampling of simulation nodes in Fig. 13 shows that the variation of effective cloud pressure, in the case of low-continuum reflectance, has very small impact on the O_2-O_2 SCD. However, it is theoretically still possible to retrieve small values (not only values close to the surface). Low sampling of simulations would result in inaccuracy of the interpolation/extrapolation. This is why the current OMI cloud LUT only exhibits high effective cloud pressure values, i.e. close to the surface pressure.

4 Implicit vs. explicit aerosol correction in the tropospheric NO_2 AMF

4.1 Tropospheric NO_2 AMF factor based on effective cloud parameters

The behaviour of the OMI cloud algorithms in response to aerosols, as analysed in Sect. 3.3, has consequences on the computation of the tropospheric NO_2 AMF. Indeed, as effective cloud parameters are sensitive to the presence of aerosols, their properties, and their location in the atmosphere, they apply an implicit aerosol correction as observed in the DOMINO product (Sect. 2). This implicit aerosol correction is obtained through the altitude-resolved AMF $a(\Psi, p)$ which uses the retrieved effective cloud fraction and cloud pressure, that are impacted by the presence of aerosols, and no explicit aerosol information. This differs from an explicit aerosol correction in which explicit aerosol parameters would be used.

Similarly to Fig. 3, Fig. 14 depicts the resulting tropospheric NO_2 AMF factor f following Eq. (5) at 439 nm, based this time on effective cloud parameters: i.e. the computation of A^{tr} is not based on τ and other aerosol properties, but on effective cloud fraction values between 0. and 0.1 and different cloud pressures. The denominator of f corresponds here to cloud-free cases (i.e. effective cloud fraction = 0). Two surface albedo values are considered (0.05 and 0.07), $\theta_0 = 25°$, $\theta = 25°$ and NO_2 profiles from TM5 in July at 12:00 p.m. (see Fig. 1). In the case of strong aerosol contamination (i.e. effective cloud fraction = 0.1), the implicit aerosol factor lies in the range of 1.15–0.6: i.e. 15 % enhanced sensitivity if the cloud is retrieved close to the surface and likely well mixed (even below) the tropospheric NO_2 bulk; 40 % reduced sensitivity if the cloud is retrieved at elevated altitude. In cases of high τ values, the decrease of effective cloud pressure has more impact on the magnitude of f than the increase of cloud fraction. Indeed, an increase of effective cloud fraction from 0.08 to 0.1 has an impact of less than 10 %. At the same time, a change of cloud pressure from 900 to 700 hPa can induce a change of 20 % in the AMF factor.

Finally, the variability of the NO_2 profiles causes a higher variability of f, between 10 and 15 %, for cloud pressures between the surface and 700 hPa. It is highly reduced for very high clouds (i.e. cloud pressure between 300 and 500 hpa). This reduction is caused by the absence of scattering properties in the inverse cloud model which results in an almost complete mask of the tropospheric NO_2 bulk below the supposed cloud layer. This is contrary to f based on explicit aerosol properties, where even particles with strong shielding effects show a non-negligible sensitivity to the variability of tropospheric NO_2 vertical shape.

Following the sensitivity analyses of the O_2-O_2 cloud retrieval algorithm, the behaviour of tropospheric NO_2 AMFs observed in the DOMINO products, over China, can be un-

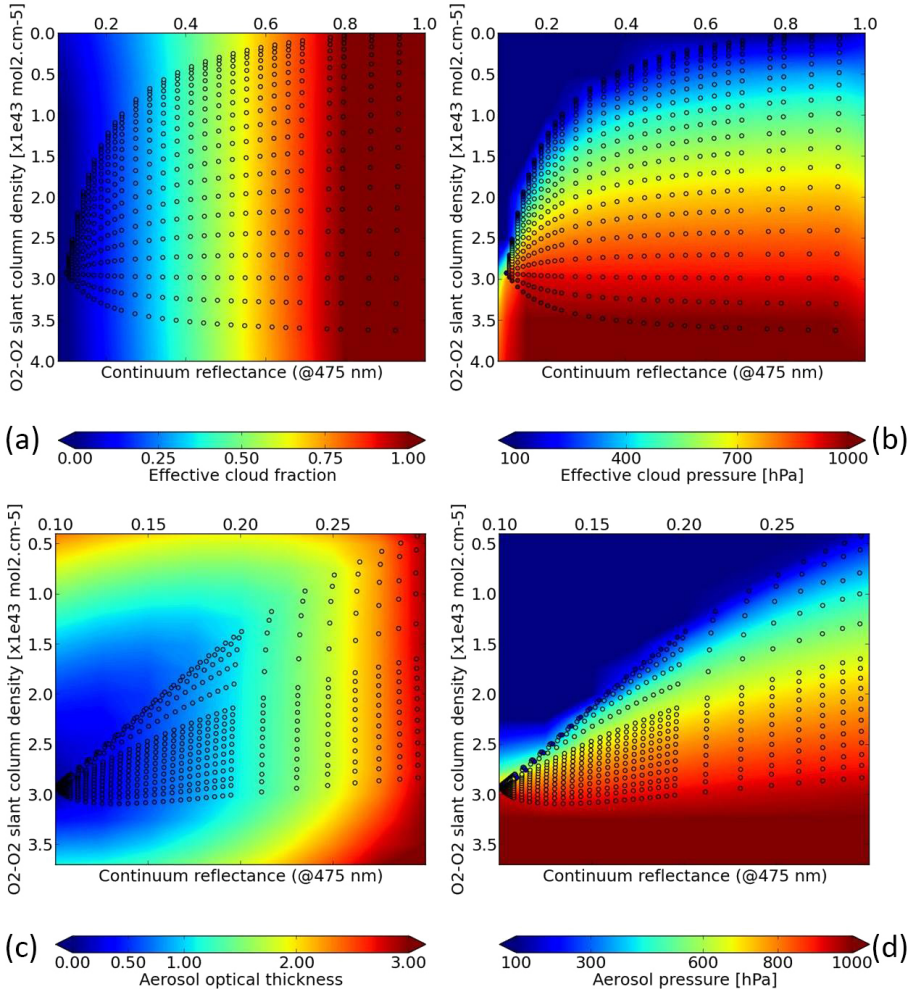

Figure 13. Effective cloud (Lambertian reflector, albedo = 0.8) and fine scattering aerosol ($\alpha = 1.5$, $\omega_0 = 0.95$, $g = 0.7$) parameters as a function of O_2-O_2 slant column density and continuum reflectance at 475 nm for the following conditions: climatology mid-latitude summer temperature, NO_2, O_3, and H_2O profiles, surface albedo = 0.05, SZA = 32°, VZA = 32°, and surface pressure = 1013 hPa. The dots are the values specified (see Table 2) in the forward simulations (named simulation nodes). The background colours result from the linear interpolation / extrapolation of the DOAS fit results: **(a)** effective cloud fraction, **(b)** effective cloud pressure [hPa], **(c)** aerosol optical thickness at 550 nm, **(d)** aerosol pressure [hPa].

derstood as follows: on average, a decrease of tropospheric NO_2 AMF in summer with increasing AOT is caused by the simultaneous increase of effective cloud fraction and decrease of effective cloud pressure. Qualitatively, this behaviour is in line with the expected aerosol shielding effect on tropospheric NO_2 in summer. Indeed, Vlemmix et al. (2015) have shown that in summer in China, aerosol particles are generally located above the tropospheric NO_2 layers. The probability that aerosol layers are located higher than tropospheric NO_2 bulks is also mentioned in other studies. For instance, Li et al. (2013) performed MAX-DOAS measurements during the PRIDE-PRD2006 campaign in the Pearl River Delta region, in China, for 4 weeks in July 2006. The considered site is located at 60 km north of Guangzhou in a rural area. It is clearly shown that (for these data) aerosol mixing layers are most often deeper/higher than NO_2 mixing layers. Mendolia et al. (2013) retrieved tropospheric NO_2 vertical column densities from OMI and MAX-DOAS measurements over Canada. One key conclusion of this work is that NO_2 diurnal profiles can even be systematically lower in summer and do not follow the expected pattern of the convective boundary layer (higher in summer than in winter). Aerosols do follow this seasonal pattern since they have a longer life time.

The absence of statistic increase/decrease of tropospheric NO_2 AMF in winter with increasing AOT is mainly caused by the smaller effective cloud fraction (compared to summer) and no variation of effective cloud pressure values which stay close to 900 hPa on average. The accuracy of the implicit aerosol correction is evaluated in the next section.

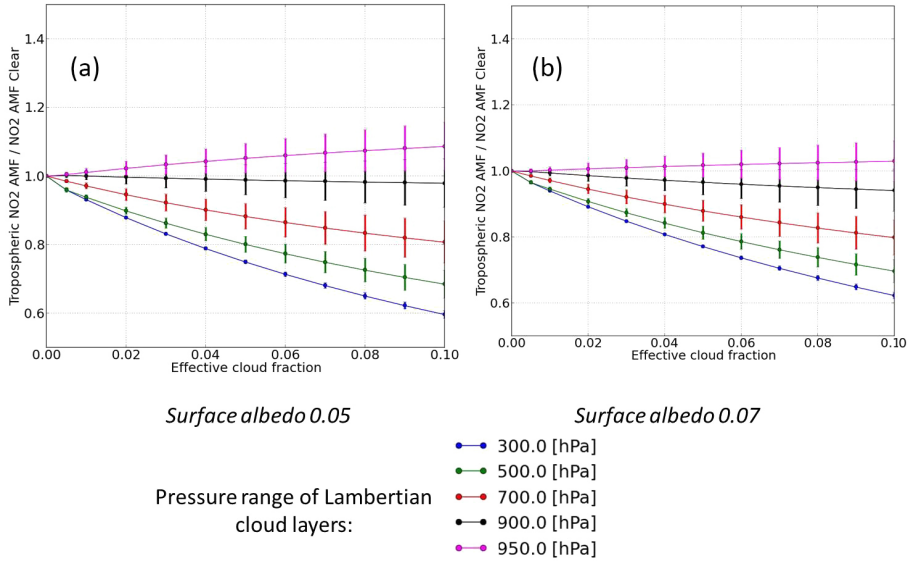

Figure 14. Tropospheric NO_2 AMF factor f at 439 nm (see Eq. 5) based on OMI effective cloud parameters (i.e. effective cloud fraction and pressure) and for two surface albedos, derived from all the NO_2 vertical profiles from TM5 simulations, 2006, East China, July (see Fig. 1). Solid lines are the average, while error bars are the standard deviation, of f computed for all the individual TM5 NO_2 profiles over this period and this region: **(a)** surface albedo 0.05, **(b)** surface albedo 0.07.

4.2 Evaluation of the implicit aerosol correction on tropospheric NO_2 AMF

In this section, AMFs computed with the cloud model used in the OMI O_2-O_2 retrieval (Sect. 3.3) are compared with AMFs computed assuming aerosols instead of clouds. This comparison is applied to cloud-free scenes dominated by aerosols. Thus, the implicit aerosol correction accuracy is here evaluated and discussed through the computation of the relative bias $S_A(\tau)$ expressed as a percentage:

$$S_A(\tau) = \frac{A^{tr}(\tau) - A^{tr}_{exp}(\tau)}{A^{tr}_{exp}(\tau)} \cdot 100\,, \quad (8)$$

where $A^{tr}_{exp}(\tau)$ is the tropospheric NO_2 AMF explicitly taking into account aerosols. This relative bias is computed in two ways: (1) assuming that $A^{tr}(\tau)$ includes an implicit aerosol correction (based on the retrieved effective cloud parameters), and (2) that no aerosol correction at all (i.e. $A^{tr}(\tau) = A^{tr}(\tau = 0)$). Then, the implicit aerosol correction can be compared to the case of no aerosol correction.

Figures 15–17 show that the relative biases S_A induced by the implicit aerosol correction vary from −10 to 30 % in most of the simulated cases. These biases are negative (i.e. underestimation of the AMFs) and minimal when aerosols are mixed with the tropospheric NO_2 bulk at the surface. They are generally positive and maximal (i.e. overestimation of the AMFs) when aerosols are elevated in the atmosphere and so not mixed with the tropospheric NO_2 peak (i.e. between 950 and 600 hPa depending on the analysed cases). In most of the simulations, the higher biases are found over scenes with elevated and high aerosol pollution, with $\tau \geq 0.6$. This is a consequence of an insufficient shielding effect applied in the computation of A^{tr} by the implicit aerosol correction through the OMI cloud algorithm. This results from too large effective cloud pressure values. When the effective cloud pressure value significantly decreases with increasing AOT, the implicit aerosol correction is then able to reproduce the aerosol shielding effect with a better accuracy. For example, in Fig. 15, when geometry angles are small ($\theta_0 = 25°$ and $\theta = 25°$), with very high aerosol pollution (τ close to 1), fine particles ($\alpha = 1.5$), and high SSA ($\omega_0 \geq 0.95$), the biases S_A decrease from 30 to around 10 %. This improvement is related to the fact that only for higher AOT is the impact on the O_2-O_2 signal sufficient to dominate over artifacts related to interpolation and limited sampling of the LUT. In cases of aerosols mixed with NO_2, the biases are likely related to the discrepancy between the opaque Lambertian cloud model and the aerosol properties.

Overall, the relative biases induced by the implicit aerosol correction are generally better than if no aerosol correction was applied in the computation of tropospheric NO_2 AMF. No aerosol correction would induce biases from −20 to 60 % on A, assuming small geometry angles ($\theta_0 = 25°$ and $\theta = 25°$) and summer NO_2 profiles (see Figs. 15 and 16). Assuming winter NO_2 profiles (e.g. Fig. 17a) or larger angles (e.g. $\theta_0 = 50°$ in Fig. 17c), these relative biases can even increase up to 150 % depending on the aerosol altitude. Indeed, in those cases, aerosols apply a stronger shielding effect on the tropospheric NO_2 bulk.

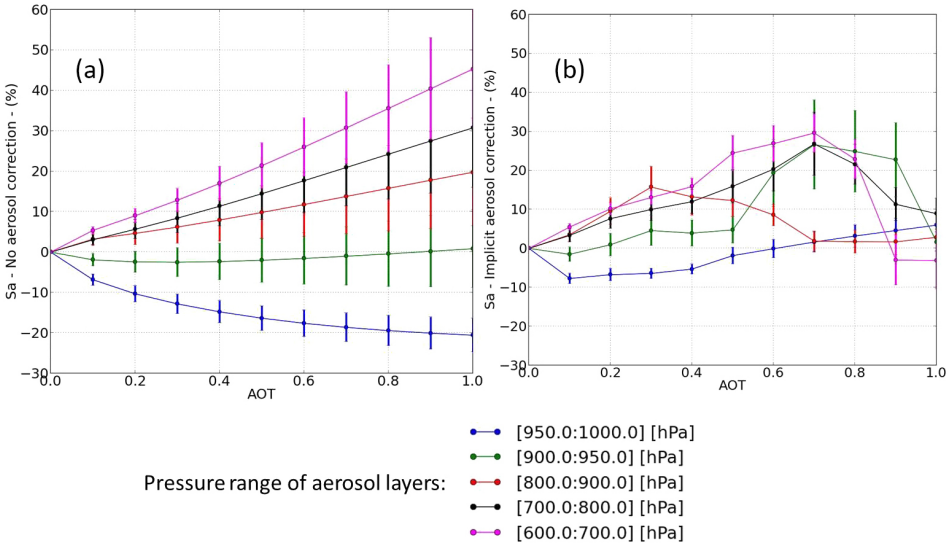

Figure 15. Comparison of relative tropospheric NO_2 AMF biases S_A at 439 nm (see Eq. 8) assuming different aerosol layers, surface albedo = 0.05, SZA = 25°, VZA = 25°, and TM5 NO_2 vertical profiles for the month of July at 12:00 p.m. over China (see Fig. 1). Aerosol properties are defined by Ångström coefficient = 1.5, SSA = 0.95, and asymmetry parameter = 0.7. Solid lines are the average, while error bars are the standard deviation, of S_A computed for all the individual TM5 NO_2 profiles over this period and this region: **(a)** S_A assuming no aerosol correction, **(b)** S_A assuming implicit aerosol correction through the OMI cloud retrieval algorithm.

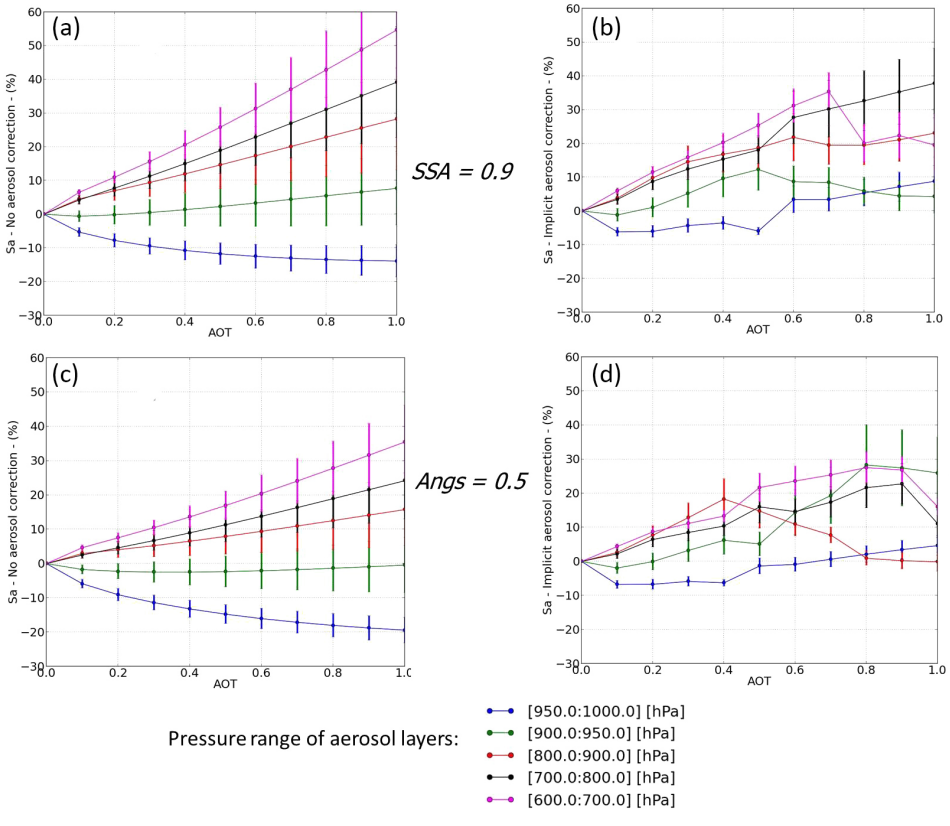

Figure 16. Similar to Fig. 14 but with different aerosol SSA and Ångström coefficient values: **(a)** S_A assuming no aerosol correction, SSA = 0.9, **(b)** S_A assuming implicit aerosol correction through the OMI cloud retrieval algorithm, SSA = 0.9, **(c)** S_A assuming no aerosol correction is applied, Ångström coefficient = 0.5, **(d)** S_A assuming implicit aerosol correction through the OMI cloud retrieval algorithm, Ångström coefficient = 0.5.

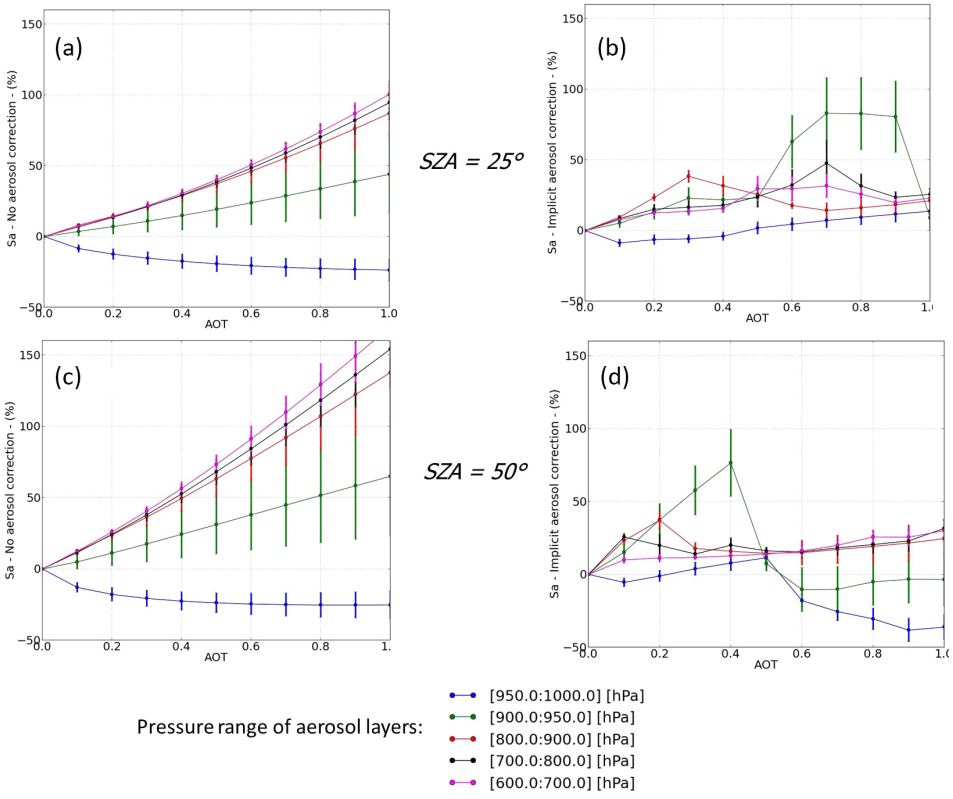

Figure 17. Similar to Fig. 14 but with NO_2 profiles for January and SZA = 50°: **(a)** S_A assuming no aerosol correction is applied, January NO_2 profiles, **(b)** S_A assuming implicit aerosol correction through the OMI cloud retrieval algorithm, January NO_2 profiles, **(c)** S_A assuming no aerosol correction is applied, aerosols, January NO_2 profiles and SZA = 50°, **(d)** S_A assuming implicit aerosol correction through the OMI cloud retrieval algorithm, January NO_2 profiles and SZA = 50°.

Aerosol altitude and amount (i.e. AOT) are the key drivers of the magnitude of the relative biases S_A. Effects of aerosols microphysics, such as associated SSA or size, have a second order of magnitude. Compared to Fig. 15, Fig. 16 shows that coarser particles ($\alpha = 0.5$ instead of 1.5) and reduced SSA (0.9 instead of 0.95) mostly increase the relative biases induced by the implicit aerosol correction for very large AOT ($\tau \geq 1$) by increasing values from around 10 to 40 %. However, these values still remain lower than if no aerosol correction was applied: S_A values are close to 55 % in the case of high aerosol altitude. For lower AOT values, no significant changes are visible. Figure 16 depicts that the shape of NO_2 vertical profile and large angles do not significantly change the S_A values of implicit aerosol corrections for elevated aerosol layers (from 900 to 600 hPa). Only in the specific case of aerosols located between 900 and 950 hPa are the values increased (between 50 and 70 %). The cause is an enhancement effect produced by too large effective cloud pressure while aerosols actually apply a strong shielding effect.

The monthly variability of the NO_2 profile shape induces a variability on the relative biases for implicit aerosol correction between 10 and 20 % (indicated by the error bars in Figs. 14–16). The magnitude of this variability depends on the distance between the aerosol layer and the peak of the tropospheric NO_2 bulk. It is generally larger when the aerosol layer is close to the maximum in the NO_2 profiles.

Relative biases associated with implicit aerosol correction shows an irregular behaviour with respect to increasing AOT values: i.e. they do not smoothly increase or decrease with increasing AOT. They somewhat either increase or decrease depending on AOT (and aerosol altitude) values. This differs from the smooth increase of relative biases assuming no aerosol correction with respect to AOT. This is probably caused by the coarse sampling of the designed cloud LUT combined with the fact that the cloud model cannot describe aerosol-dominated scenes in a perfect way. A higher sampling should be designed and tested through the OMI cloud algorithm over scenes dominated by aerosols. The behaviour of these biases could lead to complex spatial and temporal patterns of the individual DOMINO tropospheric NO_2 products over highly polluted areas, not consistent with the physical NO_2 and aerosol patterns. The potential impacts on the estimation of NO_x surface fluxes should be investigated.

4.3 Impact of the implicit aerosol correction on observed data: comparison with recent studies

An overestimation of the tropospheric NO_2 AMF results in an underestimation of the tropospheric NO_2 VCD with the same absolute magnitude according to Eq. (1). The findings here identified on the biases related to the implicit aerosol correction are consistent with those identified by Shaiganfar et al. (2011), Ma et al. (2013), and Kanaya et al. (2014). These studies found negative biases between -26 and -50 % on the OMI tropospheric NO_2 VCDs over areas with high aerosol pollution, in particular in summer. Investigations led by Ma et al. (2013) show that these underestimations can be explained by the presence of elevated aerosol layers, which are mostly observable in summer in this region (Vlemmix et al., 2015; Li et al., 2013; Mendolia et al., 2013). Very recently, Wang et al. (2015b) analysed MAX-DOAS data over Wuxi city, an area with high pollution adjoining Shanghai. It is clearly shown that, under aerosol pollution, by using the modified cloud parameters in the collocated DOMINO products, tropospheric NO_2 AMFs are overestimated. This mostly happens when the effective cloud pressure value is larger than 900 hPa.

Kuhlmann et al. (2015) recalculated tropospheric NO_2 AMFs using high-resolution aerosol parameters over the Pearl River Delta region in southern China by the Models-3 Community Multiscale Air Quality (CMAQ) modelling system. Resulting tropospheric NO_2 VCDs increased by $+6.0 \pm 8.4$ %, likely because of polluted cases where the employed aerosol and NO_2 profiles show aerosol particles located higher in altitude compared to tropospheric NO_2. In addition, Lin et al. (2014) explicitly took into account aerosol optical effects from the Goddard Earth Observing System – Chemistry (GEOS-Chem) simulations where model AOT is constrained by monthly MODIS Aqua AOT data and validated by ground-based AOT measurements. This study shows that excluding both aerosol scattering and absorption lead to changes between -40 and 90 % with AOD ≥ 0.8. Castellanos et al. (2015) have reduced the OMI NO_2 VCDs by 10 % on average by using aerosol extinction vertical profile observations from the Cloud–Aerosol Lidar with Orthogonal Polarization (CALIOP) instrument and AOD and SSA from the OMI/Aura level-2 near UV Aerosol (OMAERUV) database for scenes over South America including absorbing biomass-burning aerosols. According to the figures of CALIOP and collocated Tracer Model 4 (TM4) NO_2 profiles, the processed cases seem to include aerosol particles mixed (in parts) with the tropospheric NO_2 bulk. Finally, the new Peking University OMI NO_2 (POMINO) data set which takes aerosol properties from GEOS-Chem simulations, and which is based on the reprocessing of all the DOMINO product, show on average a reduction of the tropospheric NO_2 VCDs by 0–40 % over most of China (Lin et al., 2015). However, it is mentioned that individual reductions or enhancements depend strongly on location and season, and thus on the occurrence of the relative altitude between aerosol particles and tropospheric NO_2.

Overall, all these references which performed real retrievals show consistent numbers and conclusions with the sensitivity study performed here, and highlight the crucial role played by the actual OMI cloud algorithm and the derived implicit aerosol correction. This emphasizes that high aerosol pollution has currently large impacts on the individual OMI tropospheric NO_2 products over industrialized regions and cloud-free scenes.

5 Conclusions

In this paper, the behaviour of the OMI cloud model over cloud-free scenes dominated by aerosols was studied as well as the accuracy of the cloud-model-based aerosol correction of tropospheric NO_2 AMFs. This study focused on the operational OMI DOMINO product for cloud-free scenes, its behaviour in the presence of aerosol-dominated scenes that were selected based on collocated MODIS Aqua aerosol products, and the comparison with numerical simulated study cases. The goals were to understand the behaviour of the implicit aerosol correction based on the OMI cloud retrieval, and to investigate how much it improves the accuracy of the tropospheric NO_2 AMFs compared to performing no correction (and assuming clear-sky conditions with no aerosols). Analyses relied on a model vs. observation approach and have specifically focused on the industrialized part of East China.

The OMI cloud algorithm cannot distinguish aerosol and cloud signals. Effective cloud parameters are retrieved over cloud-free scenes but including aerosol particles. This implies that these retrievals include considerable aerosol information (AOT, optical properties, particles size, altitude) but they are treated as an opaque Lambertian reflector (albedo of 0.8). The effective cloud fraction linearly increases with increasing AOT and can reach values between 0.1 and 0.15 for AOT $= 1$. This represents the aerosol scattering effects on the 460–490 nm continuum reflectance. The slope of the linear regression of AOT vs. cloud is, however, dependent on the aerosol properties, the surface albedo, and the SZA and VZA. The response of effective cloud pressure to aerosol scenes represents the O_2-O_2 shielding effect induced by the attenuation of photons by optically thicker aerosol layers, shortening the length of the average light path. In the case of high aerosol pollution, retrieved effective cloud pressure values correlate with the mean aerosol layer height. Values smaller than the mean aerosol layer pressure may be related to the cloud model error over aerosol scenes. In cases of low AOT or effective cloud fraction values, aerosols have little effect on O_2-O_2 absorption, leading to effective cloud pressure values close to the surface pressure independently of the altitude of the aerosol layer. This overestimation can be caused by the coarse sampling of the cloud LUT used

by the OMI cloud algorithm to convert the O_2-O_2 continuum reflectance and slant column into effective cloud fraction and pressure. Indeed, this LUT was initially intended for retrievals over cloudy scenes, not for cloud-free scenes dominated by aerosols.

Aerosols can either decrease (shielding) or increase (enhancement) the sensitivity to tropospheric NO_2 bulk. Such effects simultaneously depend on the aerosol altitude and the shape of the NO_2 vertical profile. Shielding effects mostly occur when particles are above the NO_2 layers which should mostly happen during summer in China. Generally, if no aerosol correction was performed in the DOMINO products, relative biases of the tropospheric NO_2 VCDs would range from -60 to 20 % for large AOT values. These values could even decrease to -150 % in cases of large angles (e.g. SZA $\geq 50°$) or very large vertical separation between aerosols and the tropospheric NO_2 bulk.

An implicit aerosol correction is applied in the computation of the tropospheric NO_2 AMF through the use of the retrieved effective cloud fraction and pressure over scenes dominated by aerosols. After the implicit aerosol correction, relative biases in the VCDs are negative and in the range of -40 to -20 % in the case of elevated aerosol particles and high pollution (AOT ≥ 0.6). In the case of aerosols located close to the surface or mixed with the tropospheric NO_2 bulk, relative biases in the VCDs are positive and in the range of 10 to 20 %. These values are smaller than if no aerosol correction was applied in the OMI DOMINO products. AOTs and aerosol altitude are the key drivers of these biases, while aerosol microphysical properties are of secondary importance. Note that geometry angles and shape of the NO_2 profile can either increase or decrease these values. For elevated aerosols, the main cause of these biases is an underestimation of the aerosol shielding effect by the cloud algorithm. The reason for this underestimation is probably a combination of the cloud model error, used in the presence of aerosols, and the employed numerical approach to convert the O_2-O_2 continuum reflectance and SCD into effective cloud fraction and pressure through a LUT. Furthermore, the coarse sampling in the employed cloud LUT leads to complex behaviours between these biases and AOT. An improved LUT with a higher sampling should be implemented and evaluated. The impact on the ability to estimate the NO_x surface fluxes should be further studied. The biases in the presence of aerosols located at the surface or mixed with tropospheric NO_2 are likely a consequence of the difference between the opaque Lambertian cloud model and aerosol properties.

The present analyses considered box aerosol layers (i.e. discrete atmospheric layers with constant aerosol extinction value) and assumed that aerosols cover completely the OMI pixels. It is recognized that a more realistic description of the vertical distribution of aerosols and assumptions of OMI pixels partially covered by aerosols would result in different biases. Nevertheless, biases found here compare quite well with biases found in various ground-based comparison studies. Finally, all the sensitivity studies performed here assume that, in the case of highly polluted regions, only non-explicit aerosol correction impacts the current individual OMI tropospheric NO_2 products. It should be noted that uncertainties in the shape of vertical NO_2 profile and climatology surface albedo can also play a significant role in the estimated biases when aerosols are present in the measurement.

The results described in this paper indicate that it is worthwhile to design and evaluate an improved aerosol correction in view of retrieving tropospheric NO_2 vertical column densities. This is needed in the context of OMI measurements, but even more in the future for TROPOMI (Veefkind et al., 2012). Since the spatial resolution will be higher ($7\,\text{km} \times 7\,\text{km}$), there is a significant probability that a scene will be fully covered by aerosol particles.

Acknowledgements. This work was funded by the Netherlands Space Office (NSO) under the OMI contract. The authors thank Maarten Sneep for sharing his experience with respect to the use of DISAMAR software. We are grateful to Folkert Boersma for exchanges on understanding the NO_2 and cloud products and his helpful comments related to this work. We also thank Twan von Noije and Michiel van Weele for providing the TM5 data. Finally, we thank Piet Stammes for his expertise about the aerosol simulations employed in the radiative transfer simulations and the effects on the average light path.

Edited by: L. Lamsal

References

Acarreta, J. R., De Haan, J. F., and Stammes, P.: Cloud pressure retrieval using the O_2-O_2 absorption band at 477 nm, J. Geophys. Res., 109, D05204, doi:10.1029/2003JD003915, 2004.

Boersma, K. F., Eskes, H. J., and Brinksma, E. J.: Error analysis for tropospheric NO_2 retrieval from space, J. Geophys. Res., 109, D04311, doi:10.1029/2003JD003962, 2004.

Boersma, K. F., Eskes, H. J., Veefkind, J. P., Brinksma, E. J., van der A, R. J., Sneep, M., van den Oord, G. H. J., Levelt, P. F., Stammes, P., Gleason, J. F., and Bucsela, E. J.: Near-real time retrieval of tropospheric NO_2 from OMI, Atmos. Chem. Phys., 7, 2103–2118, doi:10.5194/acp-7-2103-2007, 2007.

Boersma, K. F., Eskes, H. J., Dirksen, R. J., van der A, R. J., Veefkind, J. P., Stammes, P., Huijnen, V., Kleipool, Q. L., Sneep, M., Claas, J., Leitão, J., Richter, A., Zhou, Y., and Brunner, D.: An improved tropospheric NO_2 column retrieval algorithm for the Ozone Monitoring Instrument, Atmos. Meas. Tech., 4, 1905–1928, doi:10.5194/amt-4-1905-2011, 2011.

Bovensman, H., Burrows, J. P., Buchwitz, M., Frerick, J., Noel, S., Rozanov, V. V., Chance, K. V., and Goede, A. P. H.: SCIAMACHY: mission objectives and measurement modes, J. Atmos. Sci., 56, 127–150, 1999.

Bousserez, N.: Space-based retrieval of NO_2 over biomass burning regions: quantifying and reducing uncertainties, Atmos. Meas. Tech., 7, 3431–3444, doi:10.5194/amt-7-3431-2014, 2014.

Bucsela, E. J., Celarier, E. A., Wenig, M. O., Gleason, J. F., Veefkind, J. P., Boersma, K. F., and Brinksma, E. J.: Algorithm for NO_2 vertical column retrieval from the Ozone Monitoring Instrument, IEEE Geosci. Remote S., 44, doi:10.1109/TGRS.2005.863715, 2006.

Burrows, J. P., Weber, M., Buchwitz, M., Rozanov, V. V., Ladstädter-Weissenmayer, A., Richter, A., de Beek, R., Hoogen, R., Bramstedt, K., Eichmann, K.-U., Eisinger, M., and Perner, D.: The Global Ozone Monitoring Experiment (GOME): mission concept and first scientific results, J. Atmos. Sci., 56, 151–175, 1999.

Castellanos, P., Boersma, K. F., Torres, O., and de Haan, J. F.: OMI tropospheric NO_2 air mass factors over South America: effects of biomass burning aerosols, Atmos. Meas. Tech., 8, 3831–3849, doi:10.5194/amt-8-3831-2015, 2015.

Curier, R. L., Kranenburg, R., Segers, A. J. S., Timmermans, R. M. A., and Schaap, M.: Synergistic use of OMI NO_2 tropospheric columns and LOTOS-EUROS to evaluate the NO_x emission trends across Europe, Remote Sens. Environ., 149, 58–69, doi:10.1016/j.rse.2014.03.032, 2014.

De Haan, J. F., Bosma, P. B., and Hovenier, J. W.: The adding method for multiple scattering calculations of polarized light, Astron. Astrophys., 183, 371–391, 1987.

De Haan, J. F.: DISAMAR Algorithm Description and Background Information, Royal Netherlands Meteoroligical Institute, De Bilt, the Netherlands, 1–122, 2011.

Ding, J., van der A, R. J., Mijling, B., Levelt, P. F., and Hao, N.: NO_x emission estimates during the 2014 Youth Olympic Games in Nanjing, Atmos. Chem. Phys., 15, 9399–9412, doi:10.5194/acp-15-9399-2015, 2015.

Eskes, H. J. and Boersma, K. F.: Averaging kernels for DOAS total-column satellite retrievals, Atmos. Chem. Phys., 3, 1285–1291, doi:10.5194/acp-3-1285-2003, 2003.

Hovenier, J. W. and Hage, J. I.: Relations involving the spherical albedo and other photometric quantities of planets with atmospheres, Astron. Astrophys., 214, 391–401, 1989.

Jacob, D. J., Heikes, B. G, Fan, S.-M., Logan, J. A., Mauzerall, D. L., Bradshaw, J. D., Singh, H. B., Gregory, G. L., Talbot, R. W., Blake, D. R., Sachse, G. W.: Origin of ozone and NO_x in the tropical troposphere: a photochemical analysis of aircraft observations over the South Atlantic basin, J. Geophys. Res., 101, 24235–24250, 1996.

Kanaya, Y., Irie, H., Takashima, H., Iwabuchi, H., Akimoto, H., Sudo, K., Gu, M., Chong, J., Kim, Y. J., Lee, H., Li, A., Si, F., Xu, J., Xie, P.-H., Liu, W.-Q., Dzhola, A., Postylyakov, O., Ivanov, V., Grechko, E., Terpugova, S., and Panchenko, M.: Long-term MAX-DOAS network observations of NO_2 in Russia and Asia (MADRAS) during the period 2007–2012: instrumentation, elucidation of climatology, and comparisons with OMI satellite observations and global model simulations, Atmos. Chem. Phys., 14, 7909–7927, doi:10.5194/acp-14-7909-2014, 2014.

Kleipool, Q. L., Dobber, M. R., de Haan, J. F., and Levelt, P. F.: Earth surface reflectance climatology from 3 years of OMI data, J. Geophys. Res., 113, D18308, doi:10.1029/2008JD010290, 2008.

Kuhlmann, G., Lam, Y. F., Cheung, H. M., Hartl, A., Fung, J. C. H., Chan, P. W., and Wenig, M. O.: Development of a custom OMI NO_2 data product for evaluating biases in a regional chemistry transport model, Atmos. Chem. Phys., 15, 5627–5644, doi:10.5194/acp-15-5627-2015, 2015.

Lamsal, L. N., Krotkov, N. A., Celarier, E. A., Swartz, W. H., Pickering, K. E., Bucsela, E. J., Gleason, J. F., Martin, R. V., Philip, S., Irie, H., Cede, A., Herman, J., Weinheimer, A., Szykman, J. J., and Knepp, T. N.: Evaluation of OMI operational standard NO_2 column retrievals using in situ and surface-based NO_2 observations, Atmos. Chem. Phys., 14, 11587–11609, doi:10.5194/acp-14-11587-2014, 2014.

Leitão, J., Richter, A., Vrekoussis, M., Kokhanovsky, A., Zhang, Q. J., Beekmann, M., and Burrows, J. P.: On the improvement of NO_2 satellite retrievals – aerosol impact on the airmass factors, Atmos. Meas. Tech., 3, 475–493, doi:10.5194/amt-3-475-2010, 2010.

Levelt, P. F., Hilsenrath, E., Leppelmeier, G. W., van den Oord, G. H. J., Bhartia, P. K., Tamminen, J., de Haan, J. F., and Veefkind, J. P.: Science objectives of the Ozone Monitoring Instrument, IEEE T. Geosci. Remote, 44, 1199–1208, doi:10.1109/TGRS.2006.872336, 2006.

Li, X., Brauers, T., Hofzumahaus, A., Lu, K., Li, Y. P., Shao, M., Wagner, T., and Wahner, A.: MAX-DOAS measurements of NO_2, HCHO and CHOCHO at a rural site in Southern China, Atmos. Chem. Phys., 13, 2133–2151, doi:10.5194/acp-13-2133-2013, 2013.

Lin, J.-T., Martin, R. V., Boersma, K. F., Sneep, M., Stammes, P., Spurr, R., Wang, P., Van Roozendael, M., Clémer, K., and Irie, H.: Retrieving tropospheric nitrogen dioxide from the Ozone Monitoring Instrument: effects of aerosols, surface reflectance anisotropy, and vertical profile of nitrogen dioxide, Atmos. Chem. Phys., 14, 1441–1461, doi:10.5194/acp-14-1441-2014, 2014.

Lin, J.-T., Liu, M.-Y., Xin, J.-Y., Boersma, K. F., Spurr, R., Martin, R., and Zhang, Q.: Influence of aerosols and surface reflectance on satellite NO_2 retrieval: seasonal and spatial characteristics and implications for NO_x emission constraints, Atmos. Chem. Phys., 15, 11217–11241, doi:10.5194/acp-15-11217-2015, 2015.

Ma, J. Z., Beirle, S., Jin, J. L., Shaiganfar, R., Yan, P., and Wagner, T.: Tropospheric NO_2 vertical column densities over Beijing: results of the first three years of ground-based MAX-DOAS measurements (2008–2011) and satellite validation, Atmos. Chem. Phys., 13, 1547–1567, doi:10.5194/acp-13-1547-2013, 2013.

Maasakkers, J. D.: Vital improvements to the retrieval of tropospheric NO_2 columns from the Ozone Monitoring Instrument, Eindhoven University of Technology, Eindhoven, July 2013.

Martin, R. V., D. J. Jacob, K. Chance, T. P. Kurosu, P. I. Palmer, and M. J. Evans, Global inventory of nitrogen oxide emissions constrained by space-based observations of NO_2 columns, J. Geophys. Res., 108, 4537, doi:10.1029/2003JD003453, 2003.

Mendolia, D., D'Souza, R. J. C., Evans, G. J., and Brook, J.: Comparison of tropospheric NO_2 vertical columns in an urban environment using satellite, multi-axis differential optical absorption spectroscopy, and in situ measurements, Atmos. Meas. Tech., 6, 2907–2924, doi:10.5194/amt-6-2907-2013, 2013.

Platt, U. and Stutz, J.: Differential Optical Absorption Spectroscopy (DOAS), Principles and Applications, Springer, Berlin-Heidelberg, Germany, doi:10.1007/978-3-540-75776-4, 2008.

Remer, L. A., Kleidman, R. G., Levy, R. C., Kaufman, Y. J., Tanre, D., Mattoo, S., Martins, J. V., Ichoku, C., Koren, I., Yu, H., and Holben, B. N.: Global aerosol climatology from

the MODIS satellite sensors, J. Geophys. Res., 113, D14S07, doi:10.1029/2007JD009661, 2008.

Reuter, M., Buchwitz, M., Hilboll, A., Richter, A., Schneising, O., Hilker, M., Heymann, J., Bovensmann, H., and Burrows, J. P.: Decreasing emissions of NO_x relative to CO_2 in East Asia inferred from satellite observations, Nat. Geosci. Lett., 7, 792–795, doi:10.1038/NGEO2257, 2014.

Richter, A. and Wagner, T.: The Use of UV, in: Visible and Near IR Solar Back Scattered Radiation to Determine Trace Gases, edited by: Burrows, J. P., Platt, U., Borrell, P., The Remote Sensing of Tropospheric Composition from Space, Physics of Earth and Space Environments, Chapter 2, doi:10.1007/978-3-642-14791-3, Springer-Verlag Berlin Heidelberg, 2011.

Rozanov, V. V. and Rozanov, A. V.: Differential optical absorption spectroscopy (DOAS) and air mass factor concept for a multiply scattering vertically inhomogeneous medium: theoretical consideration, Atmos. Meas. Tech., 3, 751–780, doi:10.5194/amt-3-751-2010, 2010.

Shaiganfar, R., Beirle, S., Sharma, M., Chauhan, A., Singh, R. P., and Wagner, T.: Estimation of NO_x emissions from Delhi using Car MAX-DOAS observations and comparison with OMI satellite data, Atmos. Chem. Phys., 11, 10871–10887, doi:10.5194/acp-11-10871-2011, 2011.

Shindell, D. T., Faluvegi, G., Koch, D. M., Schmidt, G. A., Unger, N., and Bauer, S. E.: Improved attribution of climate forcing to emissions, Science, 326, 716–718, 2009.

Sneep, M., de Haan, J. F., Stammes, P., Wang, P., Vanbauce, C., Joiner, J., Vasilkov, A. P., and Levelt, P. F.: Three-way comparison between OMI and PARASOL cloud pressure products, J. Geophys. Res., 113, D15S23, doi:10.1029/2007JD008694, 2008.

Spada, F., Krol, M. C., and Stammes, P.: McSCIA: application of the Equivalence Theorem in a Monte Carlo radiative transfer model for spherical shell atmospheres, Atmos. Chem. Phys., 6, 4823–4842, doi:10.5194/acp-6-4823-2006, 2006.

Stammes, P.: Spectral radiance modelling in the UV–Visible range, in: IRS 2000: Current Problems in Atmospheric Radiation, edited by: Smith, W. L. and Timofeyev Y. M., A. Deepak, Hampton, VA, USA, 385–388, 2001.

Stammes, P., Sneep, M., de Haan, J. F., Veefkind, J. P., Wang, P., and Levelt, P. F.: Effective cloud fractions from the Ozone Monitoring Instrument: theoretical framework and validation, J. Geophys. Res., 113, D16S38, doi:10.1029/2007JD008820, 2008.

Valks, P., Pinardi, G., Richter, A., Lambert, J.-C., Hao, N., Loyola, D., Van Roozendael, M., and Emmadi, S.: Operational total and tropospheric NO_2 column retrieval for GOME-2, Atmos. Meas. Tech., 4, 1491–1514, doi:10.5194/amt-4-1491-2011, 2011.

van Noije, T. P. C., Le Sager, P., Segers, A. J., van Velthoven, P. F. J., Krol, M. C., Hazeleger, W., Williams, A. G., and Chambers, S. D.: Simulation of tropospheric chemistry and aerosols with the climate model EC-Earth, Geosci. Model Dev., 7, 2435–2475, doi:10.5194/gmd-7-2435-2014, 2014.

Veefkind, J. P., Boersma, K. F., Wang, J., Kurosu, T. P., Krotkov, N., Chance, K., and Levelt, P. F.: Global satellite analysis of the relation between aerosols and short-lived trace gases, Atmos. Chem. Phys., 11, 1255–1267, doi:10.5194/acp-11-1255-2011, 2011.

Veefkind, J. P., Aben, I., McMullan, K., Förster, H., de Vries, J., Otter, G., Claas, J., Eskes, H. J., de Haan, J. F., Kleipool, Q., van Weele, M., Hasekamp, O., Hoogeveen, R., Landgraf, J., Snel, R., Tol, P., Ingmann, P., Voors, R., Kruizinga, B., Vink, R., Visser, H., and Levelt, P.: TROPOMI on the ESA Sentinel-5 Precursor: a GMES mission for global observations of the atmospheric composition for climate, air quality and ozone layer applications, Remote Sens. Environ., 120, 70–83, doi:10.1016/j.rse.2011.09.027, 2012.

Vlemmix, T., Piters, A. J. M., Stammes, P., Wang, P., and Levelt, P. F.: Retrieval of tropospheric NO_2 using the MAX-DOAS method combined with relative intensity measurements for aerosol correction, Atmos. Meas. Tech., 3, 1287–1305, doi:10.5194/amt-3-1287-2010, 2010.

Vlemmix, T., Hendrick, F., Pinardi, G., De Smedt, I., Fayt, C., Hermans, C., Piters, A., Wang, P., Levelt, P., and Van Roozendael, M.: MAX-DOAS observations of aerosols, formaldehyde and nitrogen dioxide in the Beijing area: comparison of two profile retrieval approaches, Atmos. Meas. Tech., 8, 941–963, doi:10.5194/amt-8-941-2015, 2015.

Wagner, T., Burrows, J. P., Deutschmann, T., Dix, B., von Friedeburg, C., Frieß, U., Hendrick, F., Heue, K.-P., Irie, H., Iwabuchi, H., Kanaya, Y., Keller, J., McLinden, C. A., Oetjen, H., Palazzi, E., Petritoli, A., Platt, U., Postylyakov, O., Pukite, J., Richter, A., van Roozendael, M., Rozanov, A., Rozanov, V., Sinreich, R., Sanghavi, S., and Wittrock, F.: Comparison of box-air-mass-factors and radiances for Multiple-Axis Differential Optical Absorption Spectroscopy (MAX-DOAS) geometries calculated from different UV/visible radiative transfer models, Atmos. Chem. Phys., 7, 1809–1833, doi:10.5194/acp-7-1809-2007, 2007.

Wang, Y., Penning de Vries, M., Xie, P. H., Beirle, S., Dörner, S., Remmers, J., Li, A., and Wagner, T.: Cloud and aerosol classification for 2.5 years of MAX-DOAS observations in Wuxi (China) and comparison to independent data sets, Atmos. Meas. Tech., 8, 5133–5156, doi:10.5194/amt-8-5133-2015, 2015a.

Wang, Y., Wagner, T., Xie, P., Li, A., Beirle, S., Theys, N., Stavrakou, T., De Smedt, I., and Koukouli, M.: MAX-DOAS observations and their application to the validation of satellite and model data in Wuxi, China, 7th DOAS workshop 2015, Brussels, Belgium, 7 July 2015, doi:10.13140/RG.2.1.2379.6325, 2015b.